Fuel Cell All-Terrain Transport (FCATT) Proton Exchange Membrane (PEM) Fuel Cell Stack Failure Analysis Report

Prepared by:

Dr. Theodore Burye
Chemical Engineer
theodore.e.burye2.civ@mail.mil
Non-primary Power Systems
Ground Vehicle Power and Mobility (GVPM)
Tank Automotive Research Development and Engineering Center (TARDEC)

DISCLAIMER

Reference herein to any specific commercial company, product, process, or service by trade name, trademark, manufacturer, or otherwise, does not necessarily constitute or imply its endorsement, recommendation, or favoring by the United States Government or the Department of the Army (DoA). The opinions of the authors expressed herein do not necessarily state or reflect those of the United States Government or the DoA, and shall not be used for advertising or product endorsement purposes.

DISTRIBUTION STATEMENT A. Approved for Public Release; Distribution Unlimited.

Acknowledgements

The Gas Chromatography (GC), Mass Spectroscopy (MS) and Stack Cell Voltage data were acquired from the Fuel Cell laboratory located at TARDEC in building 212B. Theodore Burye, from the Non-Primary Power Systems group, collected the GC and MS data. Benjamin Paczkowski, from the Non-Primary Power Systems group, collected the Stack Cell Voltage data.

The Scanning Electron Microscopy (SEM), Energy Dispersive Spectroscopy (EDS) and X-ray Diffraction (XRD) data were acquired from the Metallurgy laboratory located at TARDEC in building 200C. Demetrios Tzelepis and Ian Toppler, from the Characterization & Failure Analysis group, helped collect the SEM, EDS and XRD data.

The Thermo-Gravimetric Analysis (TGA) and Fourier-Transform Infrared (FTIR) Spectroscopy data were acquired from the Elastomer, Isomer, Polymer laboratory located at TARDEC in building 215. William Roland and William Bradford, from the Characterization & Failure Analysis group, collected the TGA data.

DISTRIBUTION STATEMENT A. Approved for Public Release; Distribution Unlimited.

Table of Contents

List of Tables:

List of Figures

1. Abbreviations List

ASTM: American Society for Testing and Materials

CAS: Chemical Abstracts Service

EDS: Energy Dispersive Spectroscopy

FCATT: Fuel Cell All-Terrain Transport

FTIR: Fourier-Transform Infrared

GC: Gas Chromatogram

MEA: Membrane Electrode Assembly

MS: Mass Spectrometer

NIST: National Institute of Standards and Technology

PBI: Polybenzimidazole

PEM: Proton Exchange Membrane

PWA: Phosphotungstic Acid

SEM: Scanning Electron Microscopy

TGA: Thermo-Gravimetric Analysis

XRD: X-ray Diffraction

2. Introduction

This purpose of this report is to document the results from the analysis of the Fuel Cell All-Terrain Transport (FCATT) vehicle exhaust water, prompted by an observed odor during operation. The FCATT vehicle is a Polaris utility vehicle that has been outfitted with a Proton Exchange Membrane (PEM) fuel cell.

The FCATT PEM fuel cell, under normal operating conditions, should only produce pure water and electrical power. In addition to water and electrical power, a pungent odor was detected from the FCATT fuel cell tailpipe after approximately 2 years of on-and-off use. This odor was not detectable at the time the PEM fuel cell was purchased and installed. The source of this odor was investigated, as well as other sources of degradation observed in the PEM fuel cell. The following results presented in this report will characterize the source of the odor and other degradation mechanisms, and discuss possible root causes for this degradation.

3. Experimental Operating Conditions

3.1. Introduction

During the analysis of the FCATT exhaust water odor there were three different sample types that were analyzed, which were: 1. Water, 2. Coolant, and 3. White Vinegar. Water samples were obtained from the FCATT exhaust and from laboratory experiments using deionized water. The coolant samples were obtained from the FCATT coolant system and from the original coolant container used to fill the FCATT coolant reservoir. White vinegar was used as a reference for acetic acid for samples to be compared against. The vinegar was assumed to contain 5 vol% acetic acid and will be referred to as "acetic acid" for the remainder of this report.

The FCATT exhaust water was collected and analyzed directly from the tailpipe while the PEM fuel cell stack was located inside the vehicle. After samples were collected from the vehicle the stack was removed and disassembled in the fuel cell laboratory. The top most (closest to the stack manifold), middle most, and bottom most (farthest from the stack manifold) Membrane Electrode Assembly (MEA) (the MEA included the cathode diffusion layer, cathode catalyst, proton exchange membrane, anode catalyst, and anode gas diffusion layer) sheets were characterized to determine the root cause of the odor from the exhaust water and any additional failure modes observed.

3.2. Sample Preparation and Experimental Setup

3.2.1. Gas Chromatograph and Mass Spectroscopy Preparation and Setup

To analyze the possible impacts PEM MEA sheets had on water content composition, samples needed to be prepared first.

The first samples to be tested were PEM MEA sheets that were tested in deionized water under different heating conditions to simulate different operating conditions experienced by the FCATT PEM fuel cell stack. Three 1inch x 1inch octahedral samples, shown in Figure 1, were cut from the top, middle, and bottom stack MEA sheets (shown in Figure 2) and were subjected to the following heating conditions: 1. Unheated (21°C), 2. 65°C, and 3. 95°C.

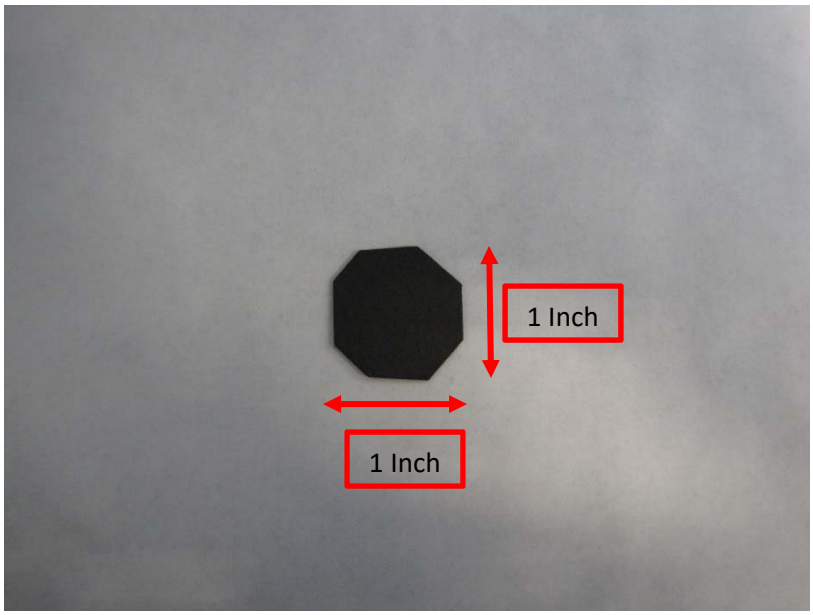

Figure 1: PEM Fuel Cell Stack Membrane Electrode Assembly Sheet Cutout.

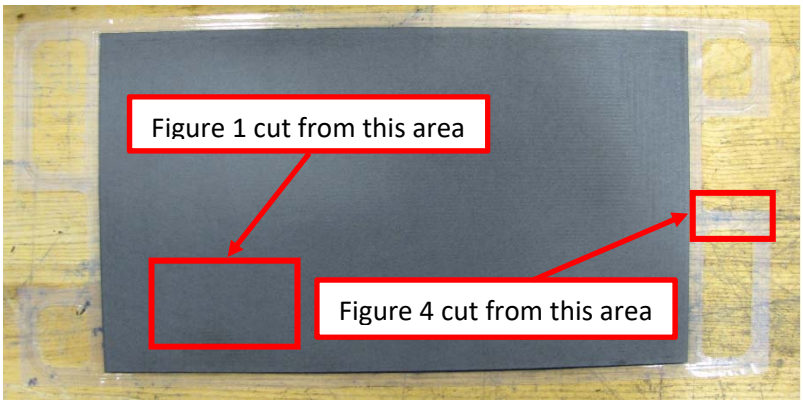

Figure 2: PEM Fuel Cell Stack Complete Membrane Electrode Assembly Sheet.

Figure 3 shows the test setup used to heat the top, middle and bottom MEA samples. Each sample was placed in a 50mL beaker that had 10mL of deionized water. A Teflon stir bar was used to hold each sample below the water line as each sample was buoyant in deionized water and it was important that the entire sample stayed in contact with the deionized water. The beaker and its contents were placed on a hotplate (Corning PC-420D) and heated to the indicated temperature for three 8-hr periods. The hotplate was not turned on for the unheated sample. The beaker was constantly monitored and

additional deionized water was added to the beaker every time the water level reach ~5mL to maintain the water level at 10mL.

Figure 3: Heating Equipment Setup.

Figure 4 shows a sample of the Proton Exchange Membrane (PEM) that was characterized using the sample approach as the MEA samples. Three PEM samples from the top, middle, and bottom MEAs to analyze the impact heat has on the PEM decomposition by itself, in contrast to the effects heat has on the MEA. Samples were obtained from the outside perimeter of the MEA sheets (where the cooling channels are located) which consists only of PEM material, shown in Figure 2. The same sample preparation was conducted on these samples as with the MEA samples and these samples were also heated using the same procedure previously used with the MEA samples.

Figure 4: Fuel Cell Membrane without Cathode or Anode.

A small sample of the FCATT tailpipe itself was also removed for analysis to determine whether it contributed to the odor being detected. The sample was placed in 10mL of deionized water and heated at 65°C (which is approximately the temperature of the water exhausting from the FCATT tailpipe) for three 8-hr periods. The tailpipe sample was also held under the deionized water using a Teflon stir bar to maximize its contact with the water.

3.3. Characterization and Analytical Techniques

3.3.1. Gas Chromatography and Mass Spectroscopy Analysis

Gas Chromatography (GC) and Mass Spectroscopy were performed using a PerkinElmer Clarus 600T GC/ Clarus 600 MS system (PerkinElmer; Waltham, MA, USA). Liquid samples were injected into the GC using an auto sampler with a 1µL injection volume, which were then passed through an Elite-1 GC column (part number N9316008) with a 0.25mm column ID, 15m column length, and 340°C maximum column temperature.

The following parameters were used for the GC and MS to characterize the following sample types. The water type applies to the FCATT exhaust water, water analyzed from the tailpipe, and water analyzed from the MEA and PEM material samples.

Water

Inlet Line Temperature: **250°C**

Mass Spectrometer Source Temperature: **230°C**

Injection Port: **A**

Injector Temperature: **120°C**

Gas Chromatograph Oven Temperature Profile:

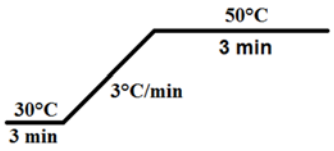

Figure 5: Water GC Oven Temperature Profile.

Gas Chromatograph Carrier Gas Flow Rate: **1.5 mL/min**

Gas Chromatograph Split Injection Mode (Flow or Ratio): **Ratio**

Gas Chromatograph Split Injection Ratio: **300:1**

Mass Spectrometer Solvent Delay: **0 min**

Mass Spectrometer Mass Number Range: **40 to 100**

FCATT Coolant

Inlet Line Temperature: **250°C**

Mass Spectrometer Source Temperature: **230°C**

Injection Port: **A**

Injector Temperature: **250°C**

Gas Chromatograph Oven Temperature Profile:

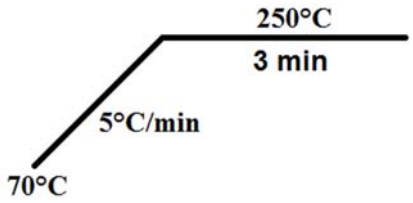

Figure 6: Coolant GC Oven Temperature Profile.

Gas Chromatograph Carrier Gas Flow Rate: **1.5 mL/min**

Gas Chromatograph Split Injection Mode (Flow or Ratio): **Split**

Gas Chromatograph Split Injection Ratio: **300:1**

Mass Spectrometer Solvent Delay: **0 min**

Mass Spectrometer Mass Number Range: **12 to 400**

Acetic Acid

Inlet Line Temperature: **250°C**

Mass Spectrometer Source Temperature: **230°C**

Injection Port: **A**

Injector Temperature: **120°C**

Gas Chromatograph Oven Temperature Profile:

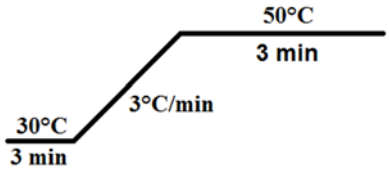

Figure 7: Acetic Acid GC Oven Temperature Profile.

Gas Chromatograph Carrier Gas Flow Rate: **1.5 mL/min**

Gas Chromatograph Split Injection Mode (Flow or Ratio): **Split**

Gas Chromatograph Split Injection Ratio: **20:1**

Mass Spectrometer Solvent Delay: **0 min**

Mass Spectrometer Mass Number Range: **40 to 100**

3.3.2. Scanning Electron Microscopy and Electron Dispersive Spectroscopy

Scanning Electron Microscopy (SEM) was performed using a Hitachi system (Hitachi; Krefeld, Germany) with an electron voltage of 30.0kV, a magnification range between 86 and 2,000, and a working distance of 10 mm. Energy Dispersive Spectroscopy (EDS) was performed using an Oxford Instruments system (Oxford Instruments; Concord, MA, USA) with an electron voltage of 30.0kV, a magnification range between 86 and 30.0k (depending on the sample type), and a working distance of 10 mm. Samples were made electronically conductive either by using copper tape or by sputtering 5.0nm of gold.

3.3.3. Particle Size Calculation

Particle size measurements were conducted using the Heyne linear intercept method [1].

3.3.4. X-Ray Diffraction

X-Ray Diffraction (XRD) was performed using a SmartLab X-ray Diffraction (XRD) system (Rigaku Americas Corporation; The Woodlands, TX, USA). Broad material scans were conducted from $10° \leq 2\theta° \leq 90°$ with a 0.040 step, 1.00°/min scan speed, a copper filament and nickel filter, and was operated at 20 kV. Focused scans around a single peak were taken from $18° \leq 2\theta° \leq 33°$ with a 0.010 step width, 0.10°/min scan speed, a copper filament and nickel filter, and was operated at 20 kV.

3.3.5. Thermo-Gravimetric Analysis

Thermo-Gravimetric Analysis (TGA) was performed using a TA Instruments TGA Q5000 system (TA Instruments; New Castle, DE, USA). Between 10.00 mg and 12.00 mg of sample was placed in a platinum pan and were heated from 21°C to 700°C using a ramp rate of 30°C/min in a nitrogen atmosphere.

3.3.6. Fourier-Transform Infrared Spectroscopy

Fourier-Transform Infrared Spectroscopy (FTIR) was performed using a Thermo Scientific Nicolet 6700 system (Thermo Scientific Instruments Corporation; Madison, WI, USA). FTIR scans were performed between 4000 and 500 cm^{-1} wavenumbers and 64 scans were performed per sample.

4. FCATT Stack Cell Voltage Profile and Exhaust Water Characterization Results

4.1. Introduction

This section will outline the characterization data collected from the FCATT PEM stack and the different types of samples analyzed by the GC/MS used for analysis of the FCATT PEM stack exhaust water. An analysis of each sample is also performed to identify the different peak assignments. The largest five to seven peaks were used for compound identification. Peaks not in the top five to seven peaks were omitted from use in compound identification because they may have occurred from slight column degradation or may be too small for accurate compound identification.

4.2. Common Mass Number Compounds

This subsection will list for reference some common mass numbers found in MS scans, and what compounds they are most likely associated with. This is not intended to be an exhaustive list and only the most common isotope for each compound will be included, as there are sometimes many isotopes for the same compound, which would make this list very lengthy.

Table 1: Common Mass Number Isotopes

Compound Name	Mass Number (m/z)
Helium Gas (He_2)	4
Methane (CH_4)	16
Water (H_2O)	18
Carbon Monoxide (CO)	28
Nitrogen Gas (N_2)	28
Methanol (CH_3OH)	32
Oxygen Gas (O_2)	32
Carbon Dioxide (CO_2)	44

4.3. Acetic Acid

Initially the pungent odor was hypothesized to be acetic acid due to the smell being similar to vinegar. If acetic acid was found to be present in a sample then a alternate acetic acid reference was used, in addition to the National Institute of Standards and Technology (NIST) database, which was a obtained from a 5 vol% acetic acid reference sample.

Figure 8 and Figure 9 show the mass spectrogram and mass scan of the acetic acid reference sample. The reference was unheated at the time of injection and was analyzed using the parameters outlined in Chapter 3.

4.3.1. Acetic Acid GC Chromatograph and MS Scan

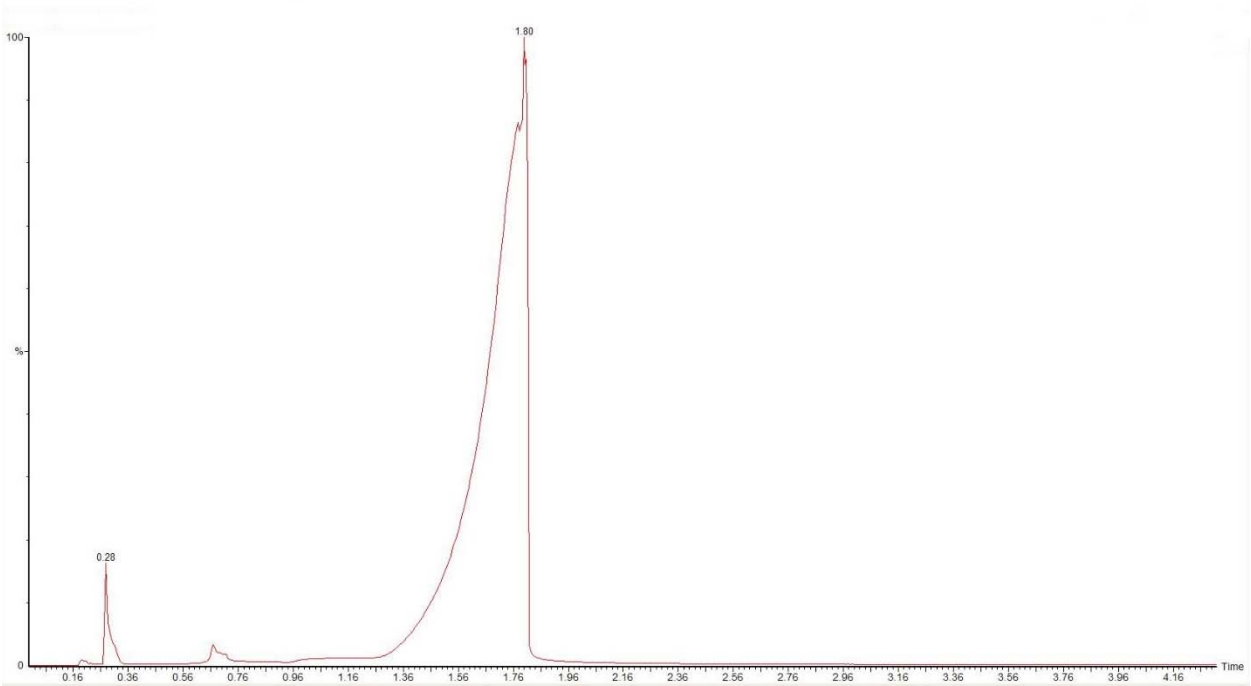

Figure 8: 5 vol% Acetic Acid Chromatogram.

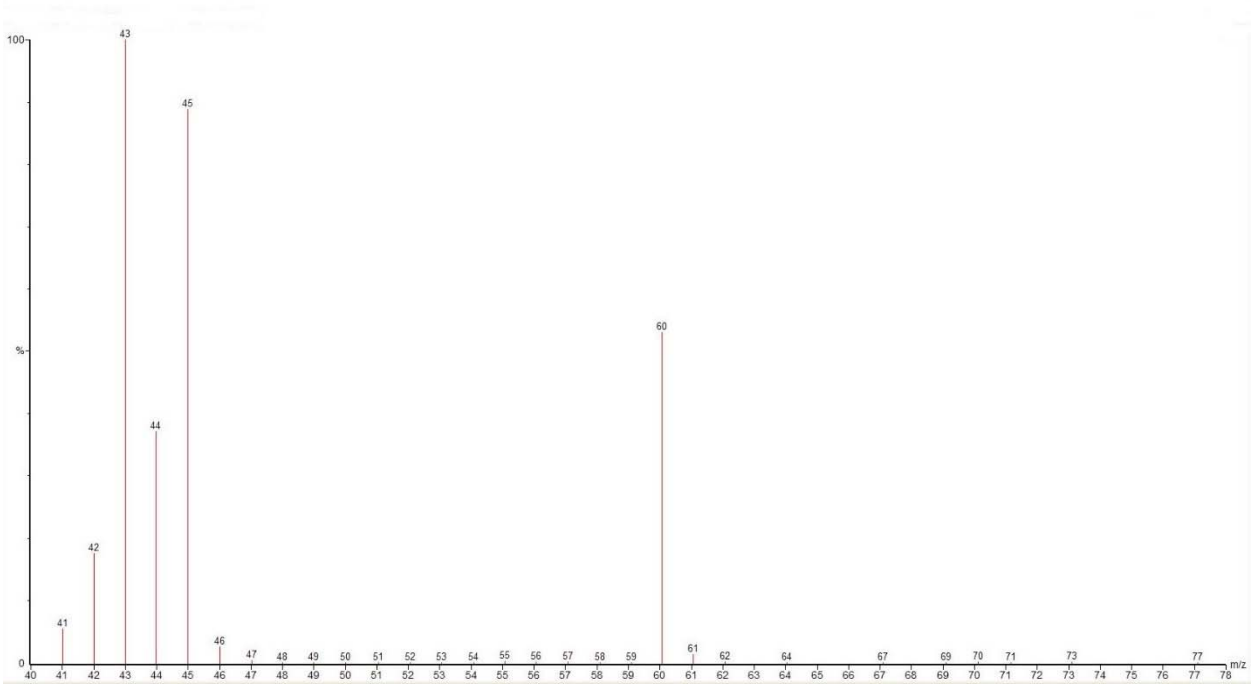

Figure 9: 5 vol% Acetic Acid MS Scan.

Figure 8 shows there are three main peaks that are identifiable using the NIST database located at 0.27min, 0.66min and 1.80min. The first peak was identified as ethyl alcohol, the second peak was ethyl acetate, and the third (and largest) peak was acetic acid. The ethyl acetate and ethyl alcohol are residual compounds from producing dilute acetic acid. A list of the Chemical Abstracts Service (CAS) registry numbers used to identify the compounds in the NIST database, where applicable, is shown below for the acetic acid.

Figure 9 shows the mass numbers for the acetic acid peak. The exact values and ratios of each of these numbers may change slightly if measured at different points in the acetic acid GC peak. The three largest mass numbers associated with acetic acid is 43, 45 and 60. The 44 mass number is also found in acetic acid but has been elevated in this example since carbon dioxide is also found in the carrier gas and has increased the value beyond what acetic acid would show.

The elution time that the acetic acid appears is important to help identify compounds found in the FCATT PEM stack exhaust water, but more importantly the mass number ratios (43, 45, and 60) between these three main peaks will help identify compounds.

4.3.1. Acetic Acid Compounds

Table 2 outlines the compounds found in the acetic acid sample shown in Figure 8 and Figure 9.

Table 2: Acetic Acid Compounds from Figure 8

Compound Name	Mass Number (m/z)	Elution Time (min)	CAS #	Origination
Ethyl Alcohol	46	0.28	64-17-5	Sample
Ethyl Acetate	88	0.66	141-78-6	Sample
Acetic Acid	60	1.80	64-19-7	Sample

.

4.3.2. Acetic Acid Concentration Variations

Variations in the concentration of acetic acid in the deionized water can manifest themselves in different ways since acetic acid is soluble in water. The following information will outline what the different GC chromatographs look like as the acetic acid molarity is increased.

Figure 10 shows the effects of acetic acid molarity on elution times. Different acetic acid molarities were analyzed, outlined in Table 3 below, to determine whether the acetic acid molarity will affect the elution time shown in Figure 8. Each scan in Figure 10 was performed using the parameters outlined in Chapter 3.

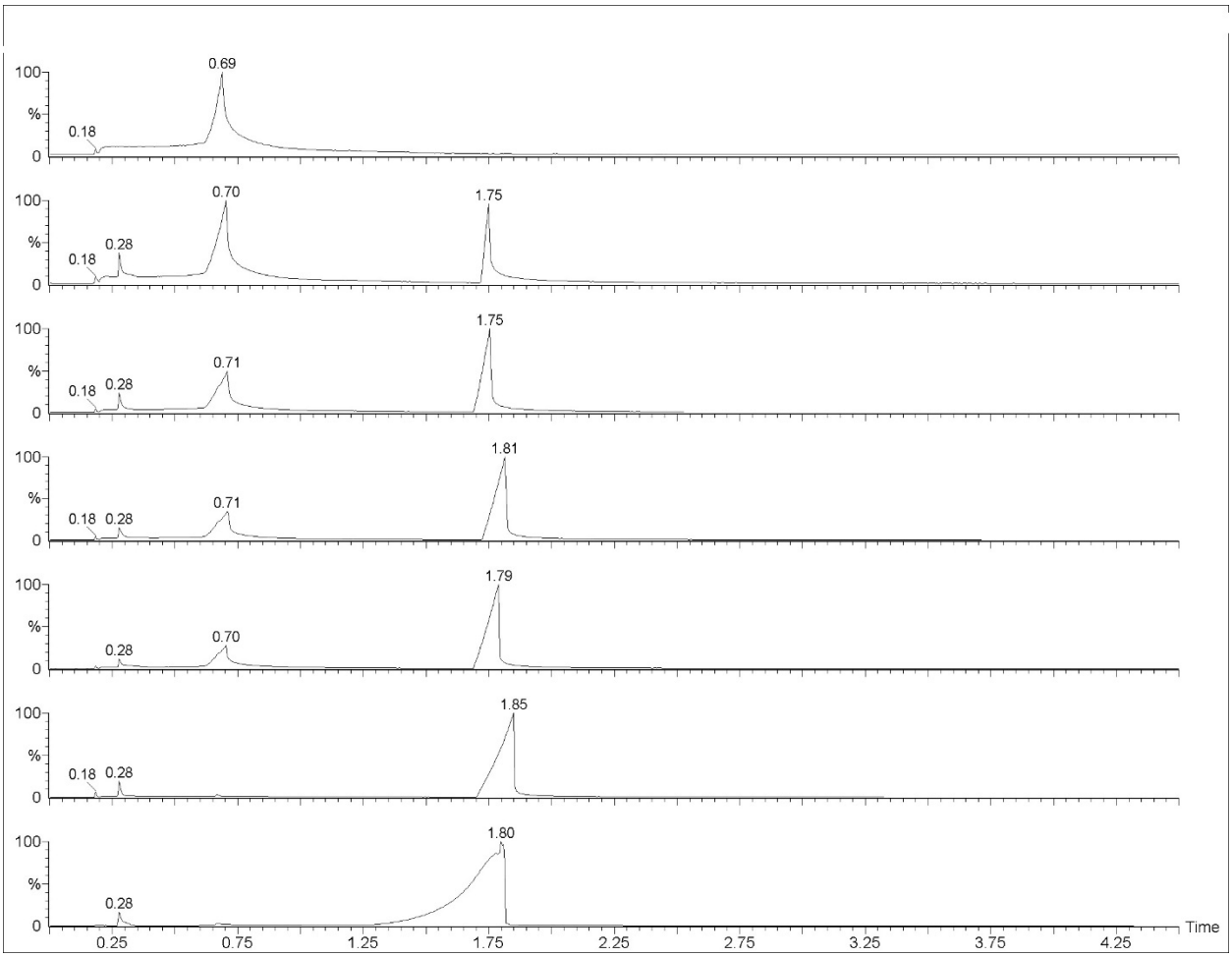

Figure 10: 5 vol% Acetic Acid Chromatograms using different solution molarities. Lowest solution molarity (top) to highest solution molarity (bottom).

Table 3: 5 vol% Acetic Acid and Deionized Water Volumes Used for Figure 10

Acetic Acid Volume (mL)	Deionized Water Volume (mL)
$5.00*10^{-3}$	$2.00*10^{2}$
$1.25*10^{-2}$	$2.00*10^{2}$
$2.50*10^{-2}$	$2.00*10^{2}$
$2.50*10^{-2}$	$6.00*10^{1}$
$2.50*10^{-2}$	$3.00*10^{1}$
$2.50*10^{-2}$	$1.00*10^{1}$
$1.00*10^{-1}$	0

As Figure 10 and Table 3 show, the peak location shown in Figure 8 stays relatively constant at higher acetic acid molarities but a second peak, not present in Figure 8, appears at lower acetic acid molarties and then grows in size as the acetic acid molarity is lowered further. In addition, the peak at 1.80min shrinks in becomes smaller and eventually disappears as the acetic acid molarity is decreased.

Analysis using the NIST database shows that both peaks (0.70min and 1.80min) are in fact acetic acid. The first peak turns out to be acetic acid dissolved in the deionized water and the second peak is acetic acid that has formed as its own phase outside the deionized water. The first peak appears to be always present, the 1.80min peak can obscure its presence when it becomes very large in size, and thus would not be noticeable in the chromatogram. A list of the CAS # number(s) used to identify the compounds in the National Institute of Standards and Technology (NIST) database, where applicable, is shown below for the acetic acid.

4.3.3. Acetic Acid Compounds using Different Concentrations

Table 4 outlines the compounds found in the acetic acid sample shown in Figure 10. If the peak is visible then “Present” will be noted, if the peak is not present or too small to detect that “Undetectable” will be noted.

Table 4: 5 vol% Acetic Acid Compounds using Different Concentrations from Figure 10

Compound Name	Mass Number (m/z)	Elution Time (min)	CAS #	Present/ Detectable
Acetic Acid Molarity = $4.37*10^{-4}$ M				
Acetic Acid in Water	60	0.70	64-19-7	Present
Acetic Acid	NA	NA	NA	Undetectable
Acetic Acid Molarity = $1.09*10^{-3}$ M				
Acetic Acid in Water	60	0.70	64-19-7	Present
Acetic Acid	60	1.75	64-19-7	Present
Acetic Acid Molarity = $2.18*10^{-3}$ M				
Acetic Acid in Water	60	0.71	64-19-7	Present
Acetic Acid	60	1.75	64-19-7	Present
Acetic Acid Molarity = $7.22*10^{-3}$ M				
Acetic Acid in Water	60	0.71	64-19-7	Present
Acetic Acid	60	1.81	64-19-7	Present
Acetic Acid Molarity = $1.43*10^{-2}$ M				
Acetic Acid in Water	60	0.70	64-19-7	Present
Acetic Acid	60	1.79	64-19-7	Present
Acetic Acid Molarity = $4.16*10^{-2}$ M				
Acetic Acid in Water	NA	NA	64-19-7	Undetectable
Acetic Acid	60	1.85	64-19-7	Present
Acetic Acid Molarity = $8.73*10^{-1}$ M				
Acetic Acid in Water	NA	NA	NA	Undetectable
Acetic Acid	60	1.80	64-19-7	Present

Next, the characterization results from the FCATT PEM stack exhaust water produced will be presented in the next section.

4.4. FCATT Combined Cathode and Anode Exhaust Water

4.4.1. FCATT Combined Cathode and Anode Exhaust Water GC Chromatograph and MS Scans

The FCATT PEM stack exhaust tailpipe contains the combined exhaust products from both the anode and cathode. Water is ideally only supposed to be produced on the cathode side of the fuel cell, but a small amount of water on the anode side was noticed to be occasionally produced too. This first analysis was to determine whether any additional peaks can be observed, besides the expected water peak.

Figure 11 shows the following scans: 1. GC chromatogram of the FCATT combined exhaust water scanned from 40-100 mass numbers (top), 2, GC chromatogram of the FCATT combined exhaust water scanned from 18-100 mass numbers (middle) and, 3. Acetic acid scanned from 40-100 mass numbers.

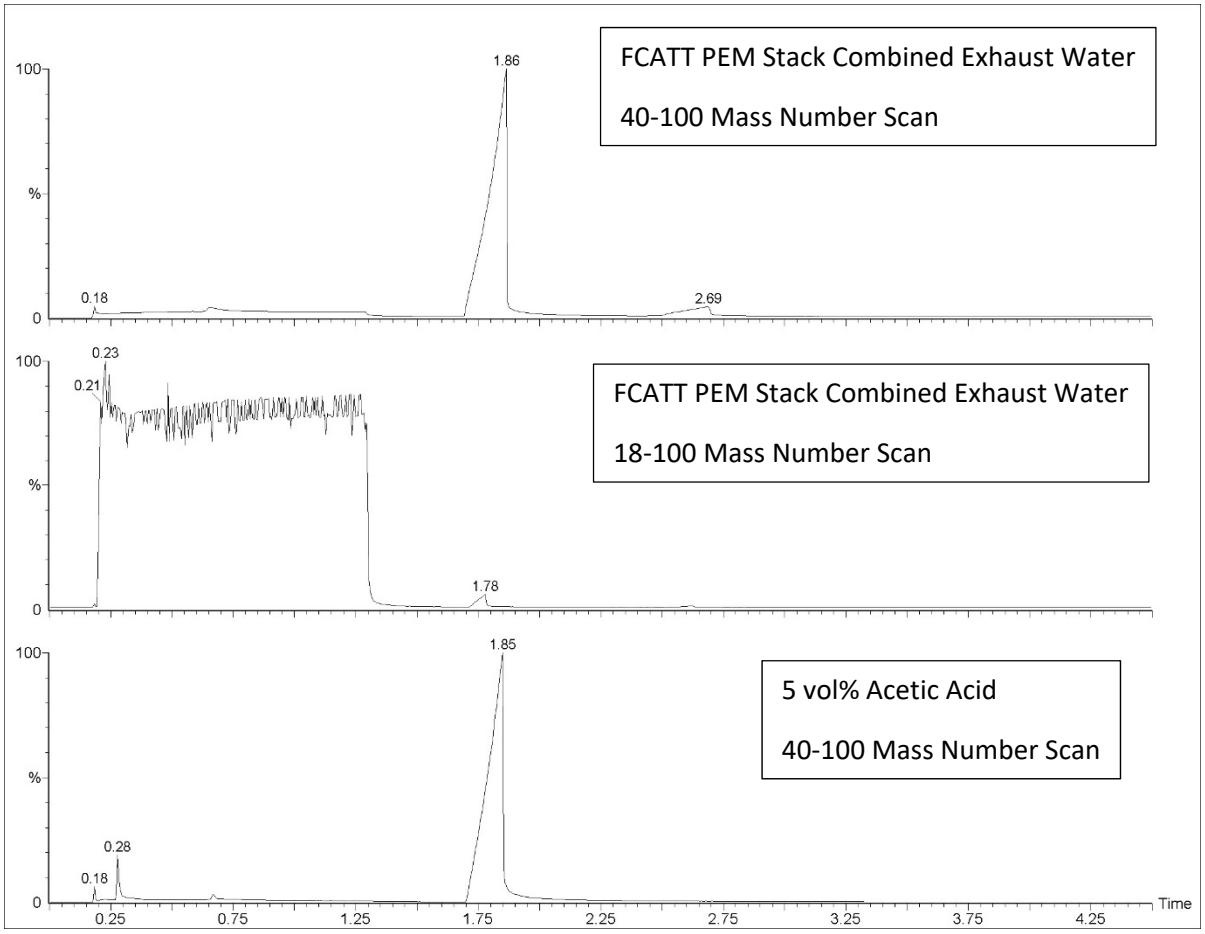

Figure 11: FCATT PEM Stack Exhaust Water (40-100 mass numbers, top), FCATT PEM Stack Exhaust Water (18-100 mass numbers, middle), and 5 vol% Acetic Acid (bottom) Chromatograms.

The initial GC analysis analyzed the FCATT PEM stack combined exhaust water from 18-100 mass numbers (middle). The large peak starting at 0.21min was from the water and also includes components found in the carrier gas (such as water, nitrogen and carbon dioxide). The second, smaller, peak at 1.78min was identified using the NIST database, with a low percentage match, as acetic acid.

To improve the NIST database match the same FCATT PEM stack water sample was scanned a second time using 40-100 mass numbers, which removed the water being detected by the MS detector. This revised scan was shown in Figure 11 (top). Using the 40-100 mass numbers resulted in the large peak starting at 0.21min to shrink in size and now only the carbon dioxide was being detected for that large peak. The peak at 1.86min was now being detected with a 93% match in the NIST database as acetic acid. The mass number ratios for acetic acid (Figure 11 bottom scan) were also compared to the mass number ratios in the FCATT combined water sample, which had a 90% match to its peak. The second peak in the top scan at 2.69min was identified with the NIST database as propionic acid, which may be the result of a side reaction occurring.

Clearly there are more compounds in the FCATT PEM stack combined exhaust water than pure water, even when the carrier gas has been removed from consideration. Acetic acid has been positively identified as well as propionic acid in the exhaust water, which are both indications that the fuel cell was not performing as intended and may have ramifications on performance later on. The next sections will be used to identify where the acetic acid was being produced and also why, through the careful examination of the FCATT coolant, FCATT tailpipe and PEM stack components (such as the MEA, cathode electrocatalyst, and anode electrocatalyst).

A list of the CAS # number(s) used to identify the compounds in the National Institute of Standards and Technology (NIST) database, where applicable, was shown below for the different samples.

4.4.2. FCATT Combined Cathode and Anode Exhaust Water Compounds

Table 5 outlines the compounds found in the MS scan of the compounds found in Figure 11. The location the compound originated at, such as in the sample or in the carrier gas, was listed in the "Origination" column in Table 5.

Table 5: Combined Concentrated Fuel Cell All-Terrain Transport (FCATT) Cathode and Anode Exhaust Water Compounds from Figure 11

Compound Name	Mass Number (m/z)	Elution Time (min)	CAS #	Origination
40-100 Mass Number FCATT PEM Stack Combined Exhaust Water Scan (top)				
Carbon Dioxide	44	0.18-1.35	NA	Carrier Gas
Acetic Acid	60	1.86	64-19-7	Sample
Propionic Acid	74	2.69	79-09-4	Sample
18-100 Mass Number FCATT PEM Stack Combined Exhaust Water Scan (middle)				
Water	18	0.18-1.35	7732-18-5	Sample
Acetic Acid	60	1.78	64-19-7	Sample
5 vol% Acetic Acid (bottom)				
Ethyl Alcohol	46	0.28	64-17-5	Sample
Ethyl Acetate	88	0.66	141-78-6	Sample
Acetic Acid	60	1.85	64-19-7	Sample

The next sections will take a look at the various compounds that make contact or possibly could make contact with the exhaust water to either produce acetic acid or add acetic acid from themselves.

4.5. FCATT Coolant

The first component to look at was the coolant used in the FCATT vehicle and was named Dynalene. The composition of the coolant was analyzed and compared to the acetic acid to determine whether acetic acid was present originally in the coolant and whether the coolant in the FCATT vehicle changed over time to acquire acetic acid, which then leaked or diffused into the cathode exhaust water stream.

Figure 12 shows the Dynalene coolant currently being used in the FCATT vehicle (top), the Dynalene coolant in the original bottle (middle), and acetic acid (bottom). As can be seen, the Dynalene in the FCATT vehicle did not change composition compared to the Dynalene in the original bottle. There was a slight decrease in elution time with the second peak (1.18 min) but all peaks are the same compositions.

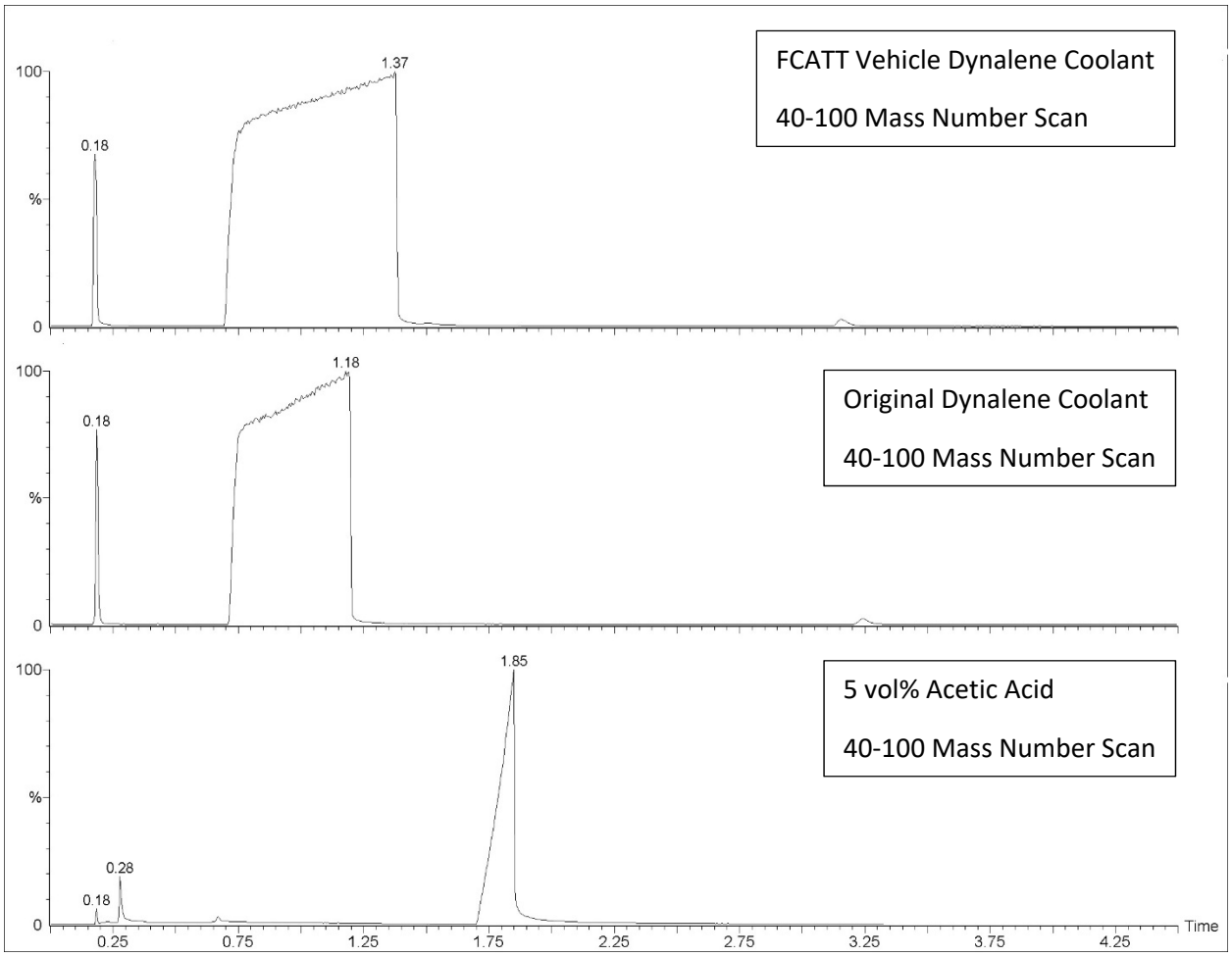

Figure 12: FCATT Vehicle Dynalene Coolant (top), Original Dynalene Coolant (middle), and 5 vol% Acetic Acid (bottom) Chromatograms.

The second observation was that there was no acetic acid peak, either dissolved in water (0.70 min) or alone (1.85 min), in the Dynalene coolant. The Dynalene coolant never contained acetic acid from the onset nor did it ever acquire acetic acid when used in the FCATT vehicle.

A list of the CAS # number(s) used to identify the compounds in the National Institute of Standards and Technology (NIST) database, where applicable, was shown below for the different samples.

4.5.1. Original and FCATT Dynalene Coolant Compounds

Table 6 outlines the compounds found in the MS scan of the compounds found in Figure 12. The location the compound originated at, such as in the sample or in the carrier gas, was listed in the "Origination" column in Table 6.

Table 6: Original and FCATT Dynalene Coolant Compounds from Figure 12

Compound Name	Mass Number (m/z)	Elution Time (min)	CAS #	Origination
FCATT Vehicle Dynalene Coolant (top)				
1,3-Propaneediol	76	0.74-1.37	504-63-2	Sample
1,3-Dioxane	88	3.15	505-22-6	Sample
Original Dynalene Coolant (middle)				
1,3-Propaneediol	76	0.74-1.18	504-63-2	Sample
1,3-Dioxane	88	3.24	505-22-6	Sample
5 vol% Acetic Acid (bottom)				
Ethyl Alcohol	46	0.28	64-17-5	Sample
Ethyl Acetate	88	0.66	141-78-6	Sample
Acetic Acid	60	1.85	64-19-7	Sample

Since the coolant did not contribute to the addition of acetic acid in the exhaust water the next area to look at was the polymer tailpipe that both the cathode and anode exhaust to. It is possible that the exhaust water was absorbing acetic acid produced by a partially decomposing polymer tailpipe.

4.6. FCATT Tailpipe

The FCATT PEM stack tailpipe, as mentioned previously, was a possible source of acetic acid production that could be absorbed into the exhaust water. The following results will compare: 1. The analysis of a piece of brand new tailpipe heated in deionized water at 65°C, 2. The FCATT PEM stack combined cathode and anode exhaust water, and 3. Acetic acid. The new tailpipe was heated to 65°C because the exhaust exiting the tailpipe while in operation was close to that temperature.

As mentioned above, the polymer tailpipe possibly could decompose slightly and produce acetic acid. The following two reactions are possible formation reactions used to produce acetic acid from a hydrocarbon chain:

$$2\ C_4H_{10} + 5O_2 \xrightarrow{Heat,Catalyst} 4\ CH_3CO_2H + 2\ H_2O \quad (1)$$

$$2\ CH_3CHO + O_2 \xrightarrow{Heat,Catalyst} 2\ CH_3CO_2H \quad (2)$$

Both possible reactions start with the oxidation of a hydrocarbon chain and oxidize the hydrocarbon using heat and catalysts to form acetic acid as a byproduct. Propionic acid, which was observed with the FCATT PEM stack combined exhaust water results, was also a side reaction observed with these two reactions. To produce high yields of acetic acid both a high heat (150°C) and catalysts are needed. These reactions still may produce acetic acid in very dilute amounts if there was no catalyst present and the applied heat was much lower.

Figure 13 shows the FCATT PEM stack combined exhaust water (top), water heated to 65°C with a new tailpipe piece (middle), and acetic acid (bottom).

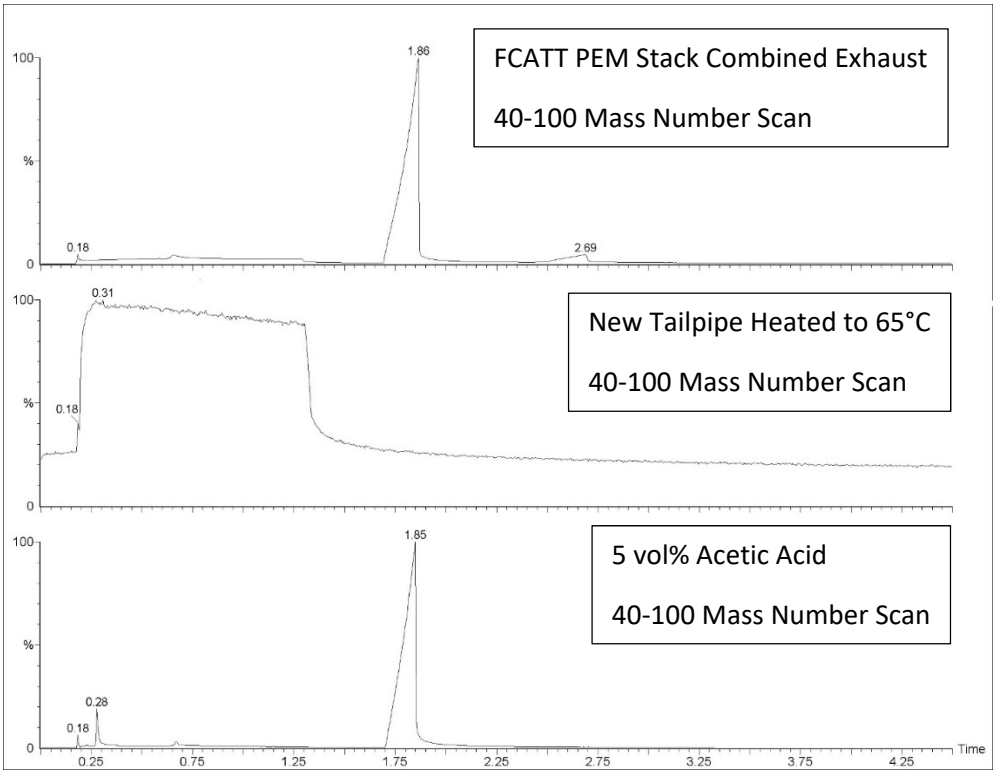

Figure 13: FCATT PEM Stack Combined Exhaust Water (top), New Tailpipe Heated (middle), and 5 vol% Acetic Acid (bottom) Chromatograms.

The results in Figure 13 show that, as previously shown, the FCATT PEM stack combined exhaust water contains an acetic acid peak at 1.86 min, but the heated new tailpipe did not produce any acetic acid peak after being submerged in deionized water and heated.

A list of the CAS # number(s) used to identify the compounds in the National Institute of Standards and Technology (NIST) database, where applicable, was shown below for the different samples.

4.6.1. FCATT Combined Exhaust Water and New Tailpipe Compounds

Table 7 outlines the compounds found in the MS scan of the compounds found in Figure 13. The location the compound originated at, such as in the sample or in the carrier gas, was listed in the "Origination" column in Table 7.

Table 7: FCATT Combined Exhaust Water and New Tailpipe Compounds from Figure 13

Compound Name	Mass Number (m/z)	Elution Time (min)	CAS #	Origination
FCATT PEM Stack Combined Exhaust Water (top)				
Carbon Dioxide	44	0.18-1.35	NA	Carrier Gas
Acetic Acid	60	1.86	64-19-7	Sample
Propionic Acid	74	2.69	79-09-4	Sample
New Tailpipe Heated (middle)				
Carbon Dioxide	44	0.18-1.35	NA	Carrier Gas
5 vol% Acetic Acid (bottom)				
Ethyl Alcohol	46	0.28	64-17-5	Sample
Ethyl Acetate	88	0.66	141-78-6	Sample
Acetic Acid	60	1.85	64-19-7	Sample

Since the tailpipe was not a source of acetic acid, and the coolant was not either, then a component in the PEM stack could be degrading and producing acetic acid. The cathode exhaust water will be separated and analyzed first, since many methods of producing acetic acid require oxygen.

4.7. FCATT PEM Stack Cathode Exhaust Water

The water produced from the cathode side of the PEM stack will be analyzed to see if a component of the cathode was contributing to the acetic acid and propionic acid production seen earlier in the FCATT PEM stack combined exhaust water chromatogram.

Figure 14 shows the chromatogram of the water analyzed from the cathode side of the fuel cell and acetic acid as a reference.

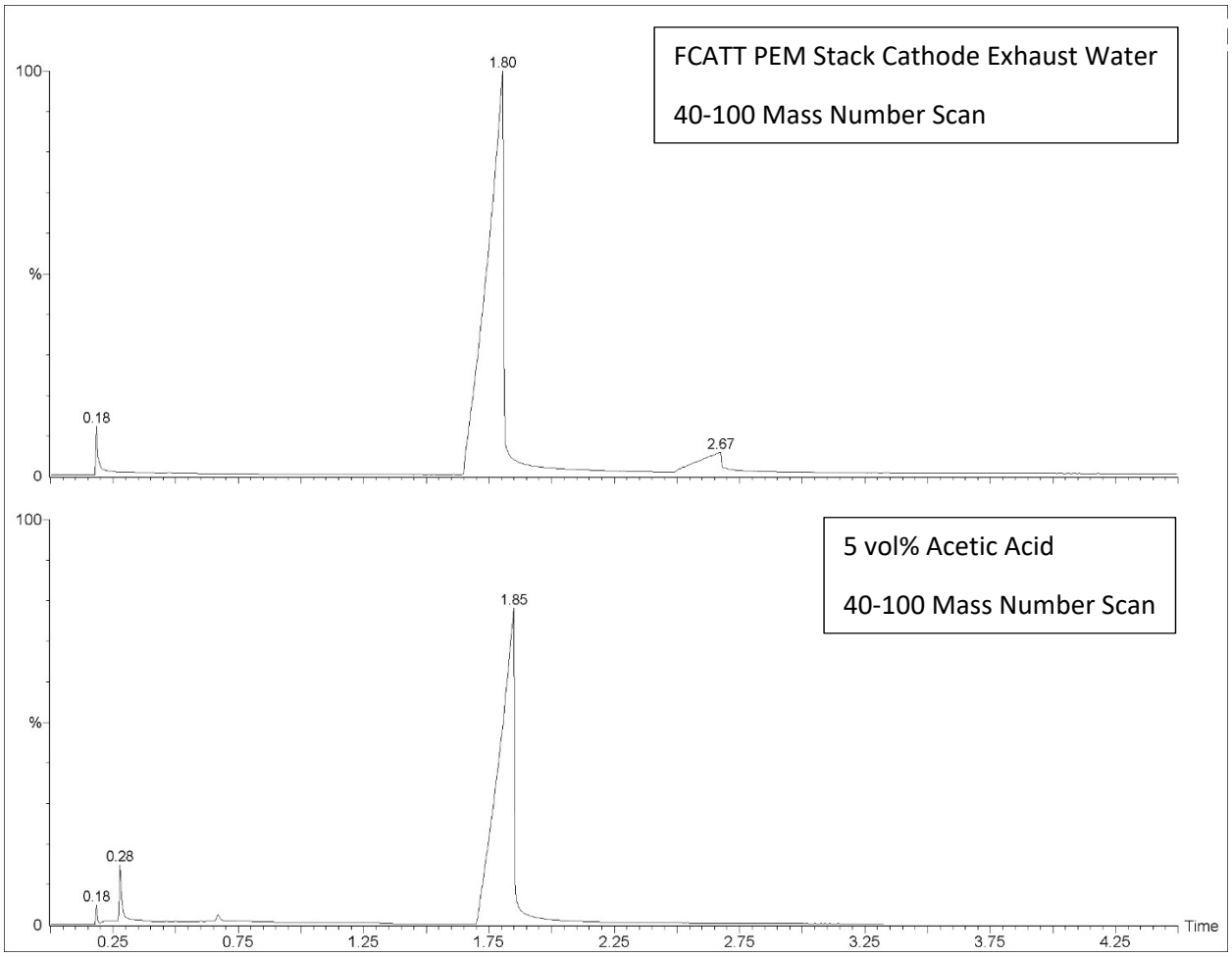

Figure 14: FCATT PEM Stack Cathode Exhaust Water (top) and 5 vol% Acetic Acid (bottom) Chromatograms.

The results in Figure 14 show the PEM stack cathode exhaust water (top) and acetic acid (bottom) are comparable and both contain acetic acid peaks. The acetic acid can be seen around 1.80-1.85min in both samples. The FCATT PEM stack cathode exhaust water has some propionic acid at 2.67 min and the acetic acid has some additional peaks from compounds used in its production.

A list of the CAS # number(s) used to identify the compounds in the National Institute of Standards and Technology (NIST) database, where applicable, is shown below for the different samples.

4.7.1. FCATT Cathode Exhaust Water Compounds

Table 8 outlines the compounds found in the MS scan of the compounds found in Figure 14. The location the compound originated at, such as in the sample or in the carrier gas, was listed in the "Origination" column in Table 8.

Table 8: FCATT PEM Stack Cathode Exhaust Water Compounds from Figure 14

Compound Name	Mass Number (m/z)	Elution Time (min)	CAS #	Origination
FCATT PEM Stack Cathode Exhaust Water (top)				
Acetic Acid	60	1.80	64-19-7	Sample
Propionic Acid	74	2.67	79-09-4	Sample
5 vol% Acetic Acid (bottom)				
Ethyl Alcohol	46	0.28	64-17-5	Sample
Ethyl Acetate	88	0.66	141-78-6	Sample
Acetic Acid	60	1.85	64-19-7	Sample

It is clear that the cathode does contribute to the formation acetic acid found in the PEM stack exhaust water. Next, the anode will also be analyzed as well to determine if any additional compounds are contributed by the anode.

4.8. FCATT PEM Stack Anode Exhaust Water

Figure 15 shows the chromatogram from the FCATT PEM stack anode exhaust water. The peak at 0.67 min was found to be acetic acid dissolved in water and the peak at 1.75 min was found to be acetic acid that had formed as a separate phase (the location of this peak can change slightly, based on concentration changes, as previous figures have shown).

Figure 16 shows the cathode exhaust water (top) compared to the anode exhaust water (bottom). Both sets of data have been shown already but here the anode acetic acid peak can be clearly seen to be significantly smaller than the cathode acetic acid peak. In addition, the anode exhaust water contains two acetic acid peaks (at 0.69min and 1.75min), where the earlier peak is acetic acid dissolved in water and the later peak is acetic acid that has formed as its own phase. Based on the results shown in Figure 10, which shows acetic acid dissolved in water occurs at lower acetic acid molarities. This reduction in acetic acid molarity on the anode side may be the results of a small leak around a seal or leakage through the PEM material. This NIST database confirms that this was acetic acid and the results presented in Figure 10 show that when the concentration of acetic acid become very dilute it only appears as a peak around 0.67-0.70 min.

Finally, as mentioned earlier, the anode half-reactions do not produce water as a byproduct. The presence of the water has been shown in literature to be the result of water back-diffusing from the cathode to the anode [2]. The acetic acid found in the anode is back-diffusing with the water from the cathode to the anode as well.

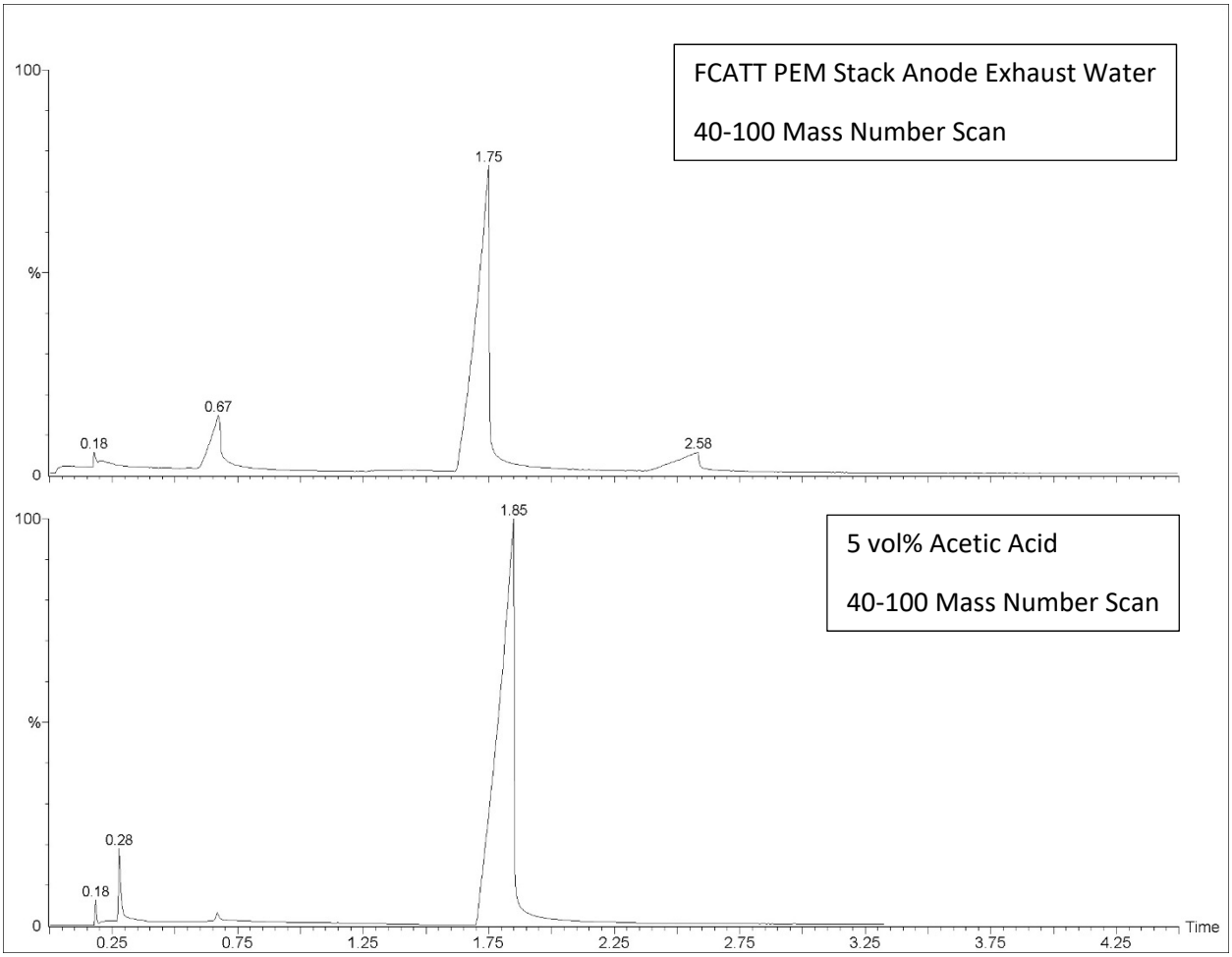

Figure 15: FCATT PEM Stack Anode Exhaust Water (top) and 5 vol% Acetic Acid (bottom) Chromatograms.

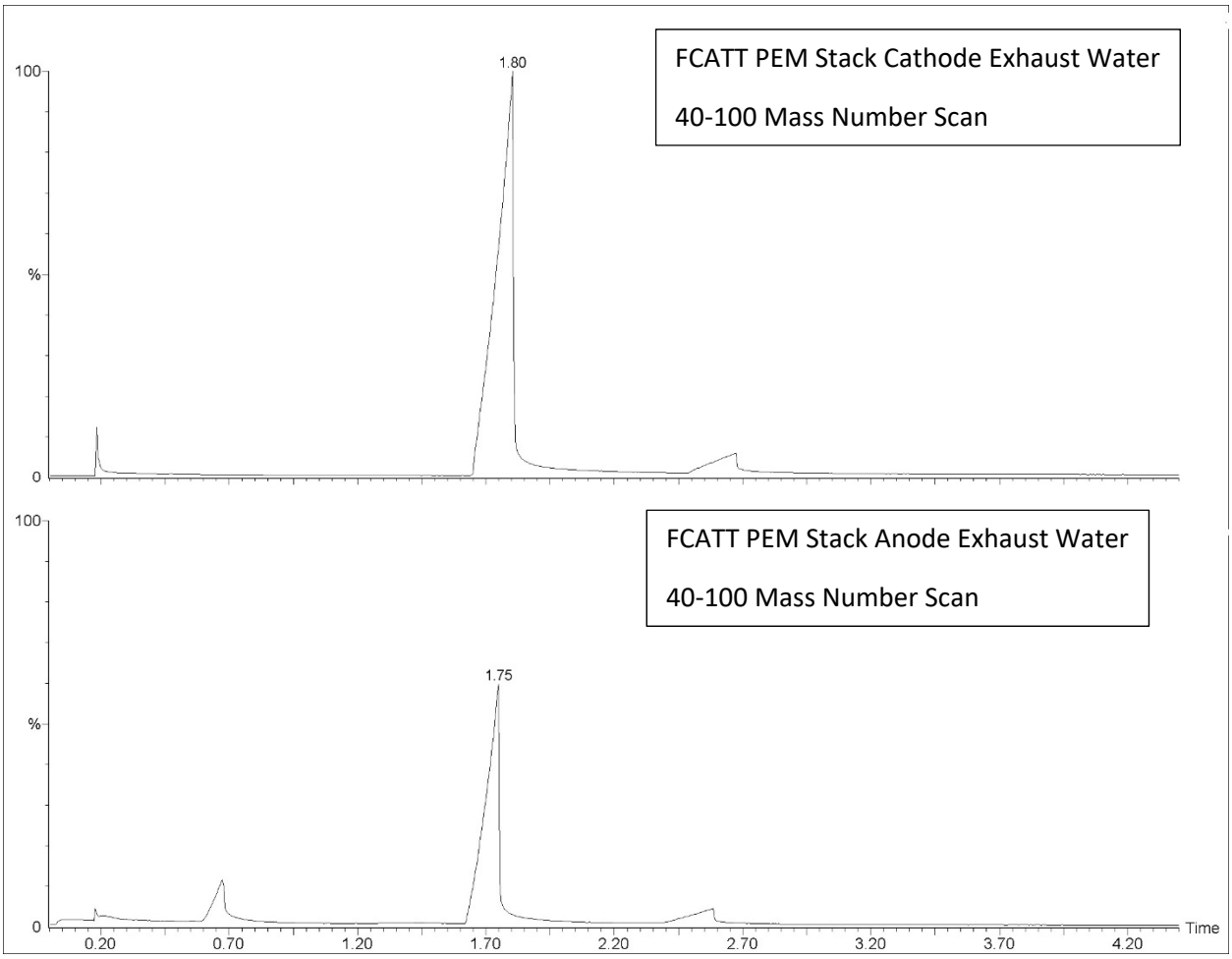

Figure 16: FCATT PEM Stack Cathode Exhaust Water (top) and Anode Exhaust Water (bottom)

A list of the CAS # number(s) used to identify the compounds in the National Institute of Standards and Technology (NIST) database, where applicable, was shown below for the different samples.

4.8.1. FCATT Anode Exhaust Water Compounds

Table 9 outlines the compounds found in the MS scan of the compounds found in Figure 15. The location the compound originated at, such as in the sample or in the carrier gas, was listed in the "Origination" column in Table 9.

Table 9: FCATT PEM Stack Anode Exhaust Water Compounds from Figure 15

Compound Name	Mass Number (m/z)	Elution Time (min)	CAS #	Origination
FCATT PEM Stack Anode Exhaust Water (top)				
Acetic Acid in Water	60	0.67	64-19-7	Sample
Acetic Acid	60	1.75	64-19-7	Sample
Propionic Acid	74	2.56	79-09-4	Sample
5 vol% Acetic Acid (bottom)				
Ethyl Alcohol	46	0.28	64-17-5	Sample
Ethyl Acetate	88	0.66	141-78-6	Sample
Acetic Acid	60	1.85	64-19-7	Sample

4.9. FCATT Stack Cell Voltage Profile

The data presented this far suggests that probably the cathode in one or more MEAs within the stack has degraded and has started to produce acetic acid and propionic acid. This was determined through the elimination of materials in proximity with the FCATT PEM stack exhaust stream that possibly could produce acetic acid. To confirm that one of more cells were degraded, the FCATT PEM stack was connected to a voltage monitoring program and cell voltages were recorded over a period of time. The operating voltages of the different cells were compared to determine whether one or multiple cells had a lower operating voltage than the average. A cell voltage significantly lower than the average could indicate that the cell was not operating at peak capacity due to degradation, and in this situation, the source of acetic acid production.

Figure 17 shows the FCATT PEM stack cell voltage profile while the stack was operating at 5.00 kWe power, which is a typical power level used when collecting the exhaust water from the FCATT tailpipe. All the cells, except Cell 1, had an average cell voltage of 0.574 V, while Cell 1 had a cell voltage of 0.320 V. Cell 1's voltage was ~44% lower than the average voltage of the other cells in the PEM stack. This amount of voltage degradation in Cell 1 is outside the normal variation of cell voltages displayed by the other cells.

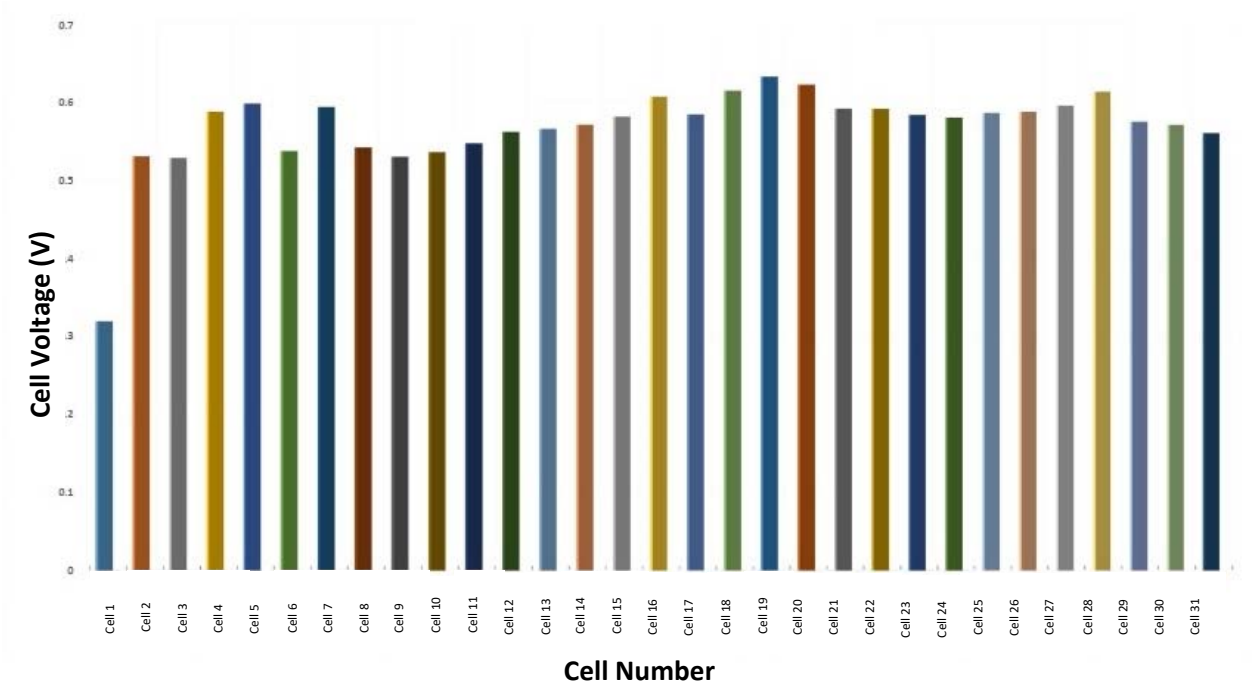

Figure 17: Initial 5.00 kWe FCATT PEM Stack Cell Voltage Profile

To check that the data presented in Figure 17 was not just a temporary anomaly, the cell voltages were recorded over a number of minutes to determine if the voltage of Cell 1 would increase and stabilize near the other cell voltages.

Figure 18 shows the same data as Figure 17 and also includes FCATT PEM stack cell voltages for a few minutes of stack operation to determine whether Cell 1's voltage remains consistently lower than the remaining cells in the stack. From the data shown in Figure 18 Cell 1 does consistently produces a significantly lower voltage than the other cells in the PEM stack. Cell 1 also displays more variation in its voltage than the other cells, but its variation in voltage never comes close to the average voltage of the stack.

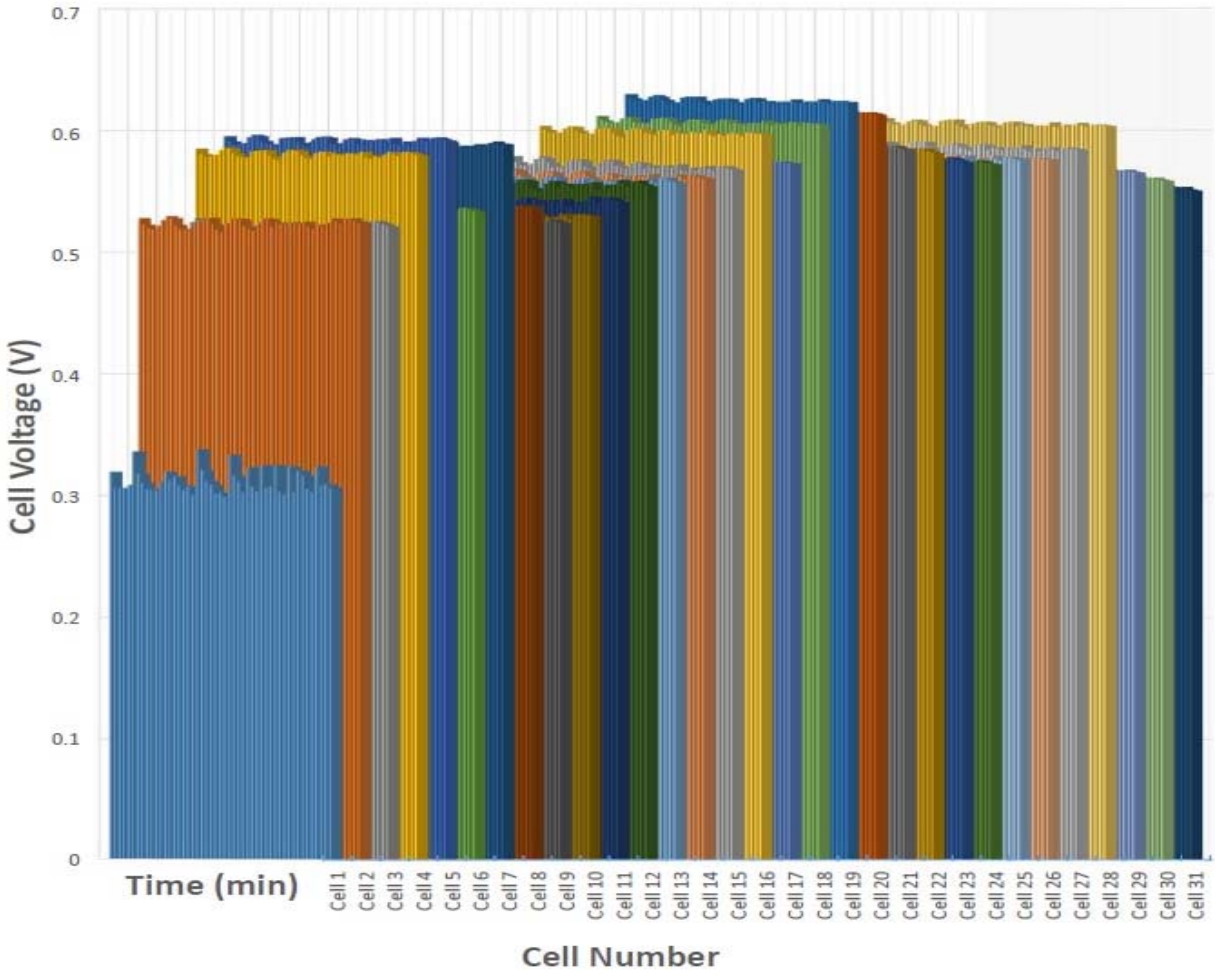

Figure 18: 5kW FCATT PEM Stack Cell Voltage Profile Over Time

Cell 1 was also the cell closest to the aluminum manifold on the PEM stack. It is possible that this reduction in operating cell voltage is due to the manifold acting as a heat sink and cooling Cell 1 and reducing its performance. To check if Cell 1's operating voltage degradation was not impacted by the manifold, and caused by other mechanisms, a second identical unused PEM stack and balance of plant (from the same company) was operating at 5.00 kWe. That data is shown below.

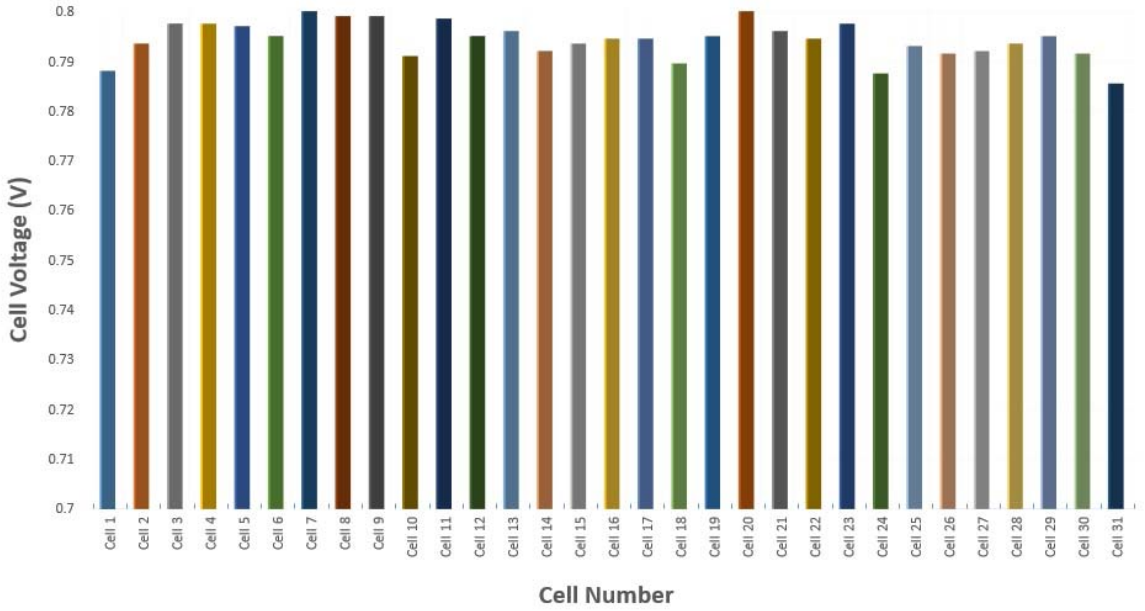

Figure 19: Unused 5 kW FCATT PEM Stack Cell Voltage Profile Initially

Figure 19 shows that Cell 1 (cell closest to the manifold), with the unused stack, still had the one of the lowest operating cell voltages from the onset of stack operation, but was much closer to the stack average operating voltage. Cell 31 had a nearly identical cell voltage compared to Cell 1, where both cells had a cell voltage ~1% lower, on average, than all the other cells in the stack. These results are not as dramatic as Figure 17, but does still show that the cell closest to the manifold consistently was tied as the lowest performing cell in the PEM stack. While Cell 31 had an aluminum backing plate attached to it, which may have contributed to its reduced cell voltage, the area of the manifold was over twice that of the backing plate. There also was piping and other balance of plant components, in addition to the manifold, which would have contributed to lowering the Cell 1 temperature significantly more than Cell 31. These results indicate that the manifold and balance of plant on the stack influenced the Cell 1 performance and over time promoted the increased voltage degradation seen in Figure 17 and Figure 18.

Based on the data presented it is clear that at least Cell 1's performance was degraded. This degradation was manifested as acetic acid production in the PEM fuel cell stack exhaust water. In addition, higher acetic acid concentrations were found in the cathode exhaust water when compared to

the anode exhaust water. The next section will investigate the root cause of this cell voltage degradation by characterizing the different components of the stack.

4.10. FCATT Stack Cell Voltage Profile and Exhaust Water Characterization Summary

Characterization of the FCATT Stack and the exhaust water showed the following information:

1. The combined cathode and anode exhaust water produced from the FCATT contained dilute acetic acid.
2. Characterization of other compounds that were in contact with the exhaust water or could leach into the exhaust water (such as the tail pipe, and FCATT coolant) were eliminated was possible sources of acetic acid.
3. Characterization of the cathode and anode exhaust water, taken separately, showed both contained acetic acid. The cathode exhaust water contained a significantly higher concentration of acetic acid than the anode exhaust water. This indicated that the FCATT PEM stack was producing the acetic acid.
4. Further investigation (using the data collected by the control software) showed that Cell 1 (the MEA closest to the manifold) had a cell voltage almost 50% lower than the other cells in the stack, which indicates degradation. The cell degradation was hypothesized to be influenced by the manifold and balance of plant components next to Cell 1.

5. PEM Stack Membrane Exchange Assembly and Proton Exchange Membrane Characterization

5.1. Introduction

This section will investigate primarily what components in the PEM stack is producing acetic acid. Before discussing the data collected an introduction into which PEM stack components are being tested will be presented.

The PEM stack was composed of multiple cells, mentioned in Section 4.9. Each cell is composed of the anode gas diffusion layer, anode electrocatalyst, proton exchange membrane (PEM) (transports protons from the anode to cathode), cathode electrocatalyst, and cathode gas diffusion layer. The entire cell is also referred to the Membrane Exchange Assembly (MEA). The MEA closest to the stack manifold was Cell 1 and the MEA furthest away from the stack manifold was Cell 31, both shown in Section 4.9.

This chapter will characterize the MEA and the PEM material to determine if either were a contributor to the acetic acid produced in the FCATT PEM stack exhaust water shown in Chapter 4. The next section will take three MEA sample pieces (samples will be taken from Cells 1, 20 and 31. Sample size was shown in Figure 1) and heat them to the same operating temperature (~65°C) as the PEM stack to determine whether similar results can be produced as in Chapter 4. Varying operating temperatures, above and below the typical operating temperature, were also used to investigate if temperature has an impact on the results. Since a wide range of acetic acid elution times, based on different molarity values, have already been provided, the following sets of data will not compare MEA and PEM material test data against acetic acid references.

5.2. Heated PEM Stack Membrane Electrode Assembly

Figure 20 through Figure 22 show the water composition after heating MEA samples from Cells 1 (top), 20 (middle) and 31 (bottom) in deionized water for three 8-hr periods at: 1. room temperature (21°C) (Figure 20), 2. 65°C (Figure 21) and 3. 95°C (Figure 22). Acetic acid dissolved in the deionized water eluted between 0.61-0.65min and acetic acid that formed as a separate phase eluted around 1.68min.

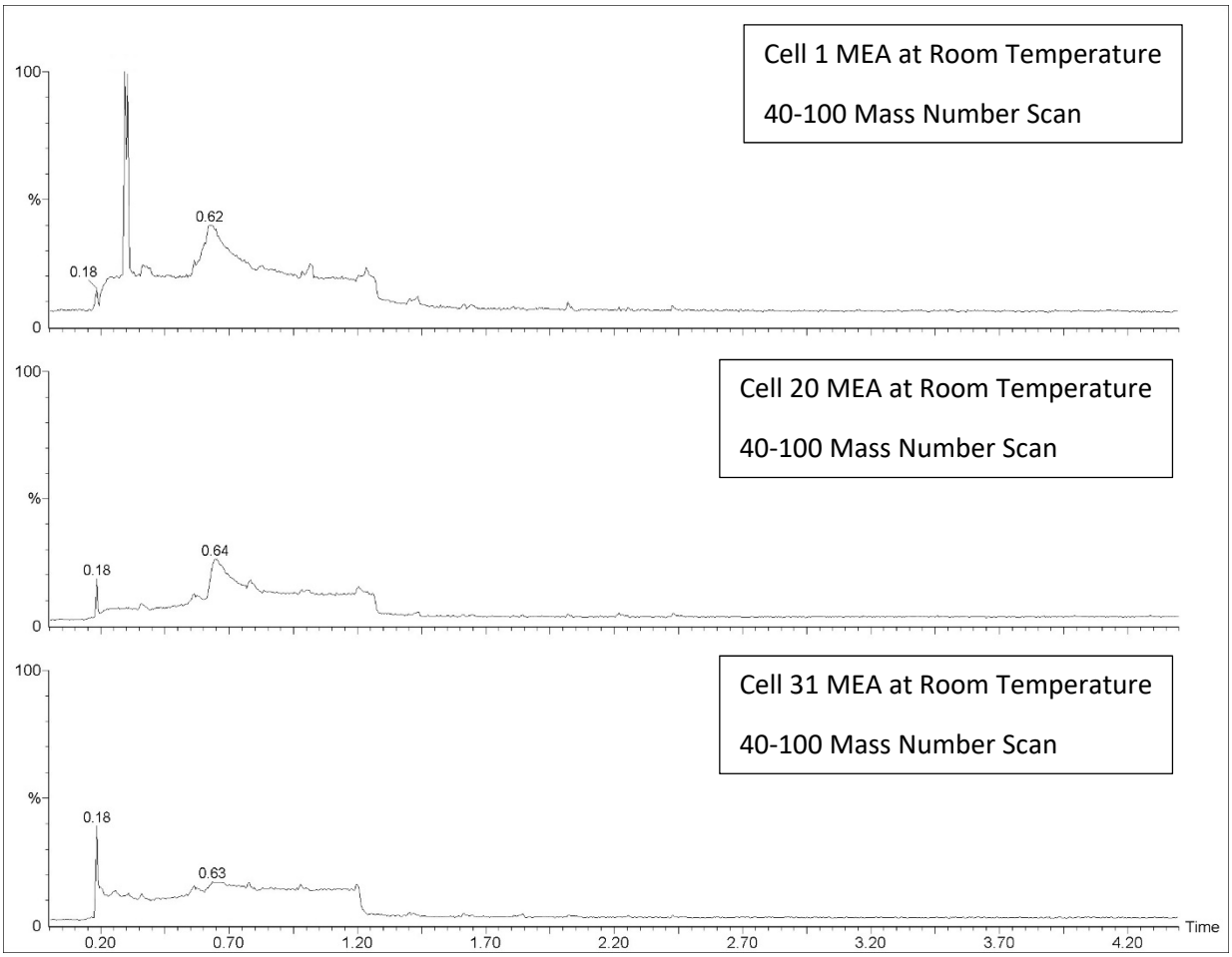

Figure 20: PEM Stack Membrane Electrode Assembly's (MEA) for Cell 1 (top), Cell 20 (middle) and Cell 31 (bottom) at Room Temperature Chromatograms.

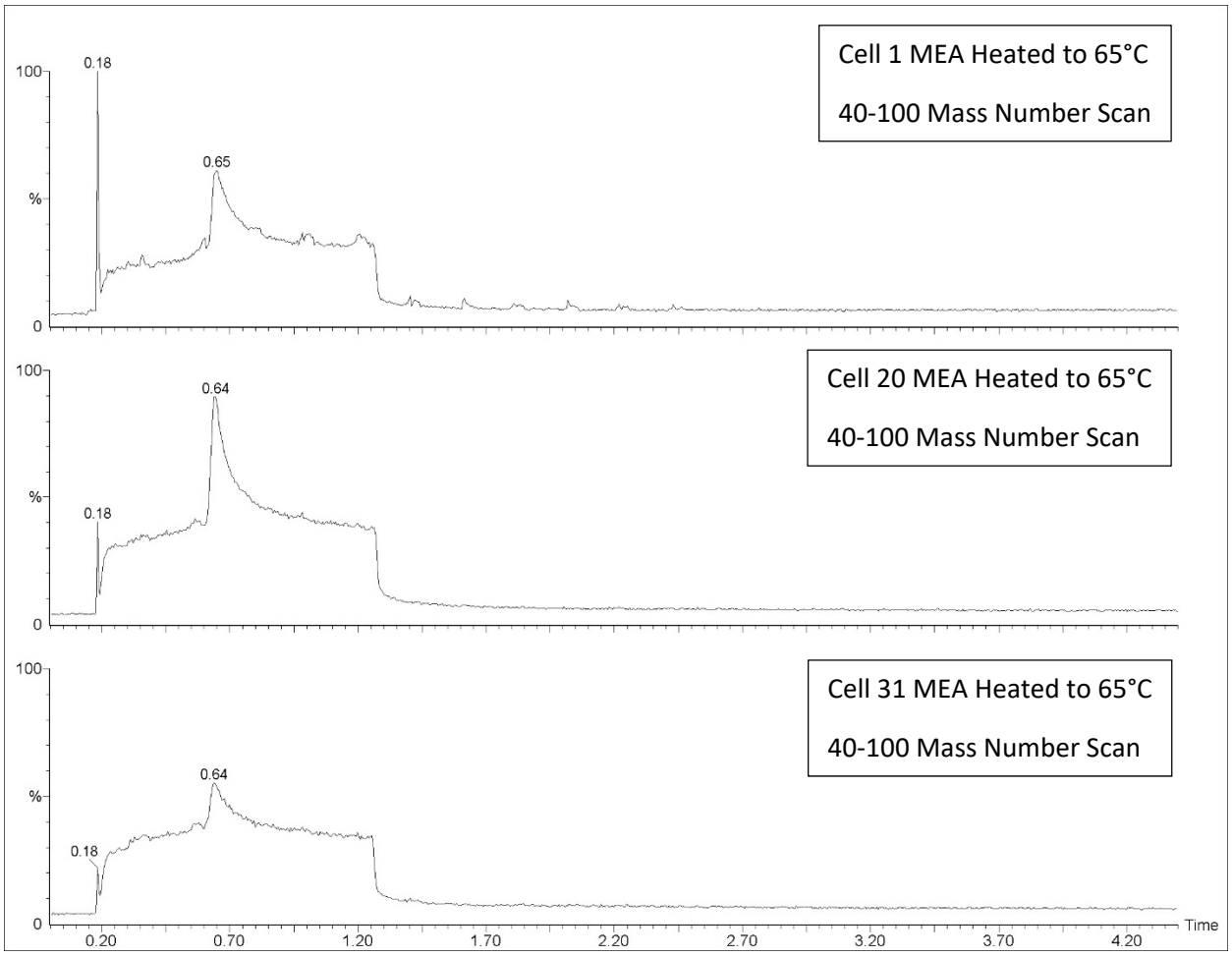

Figure 21: PEM Stack Membrane Electrode Assembly's (MEA) for Cell 1 (top), Cell 20 (middle) and Cell 31 (bottom) Heated to 65°C Chromatograms.

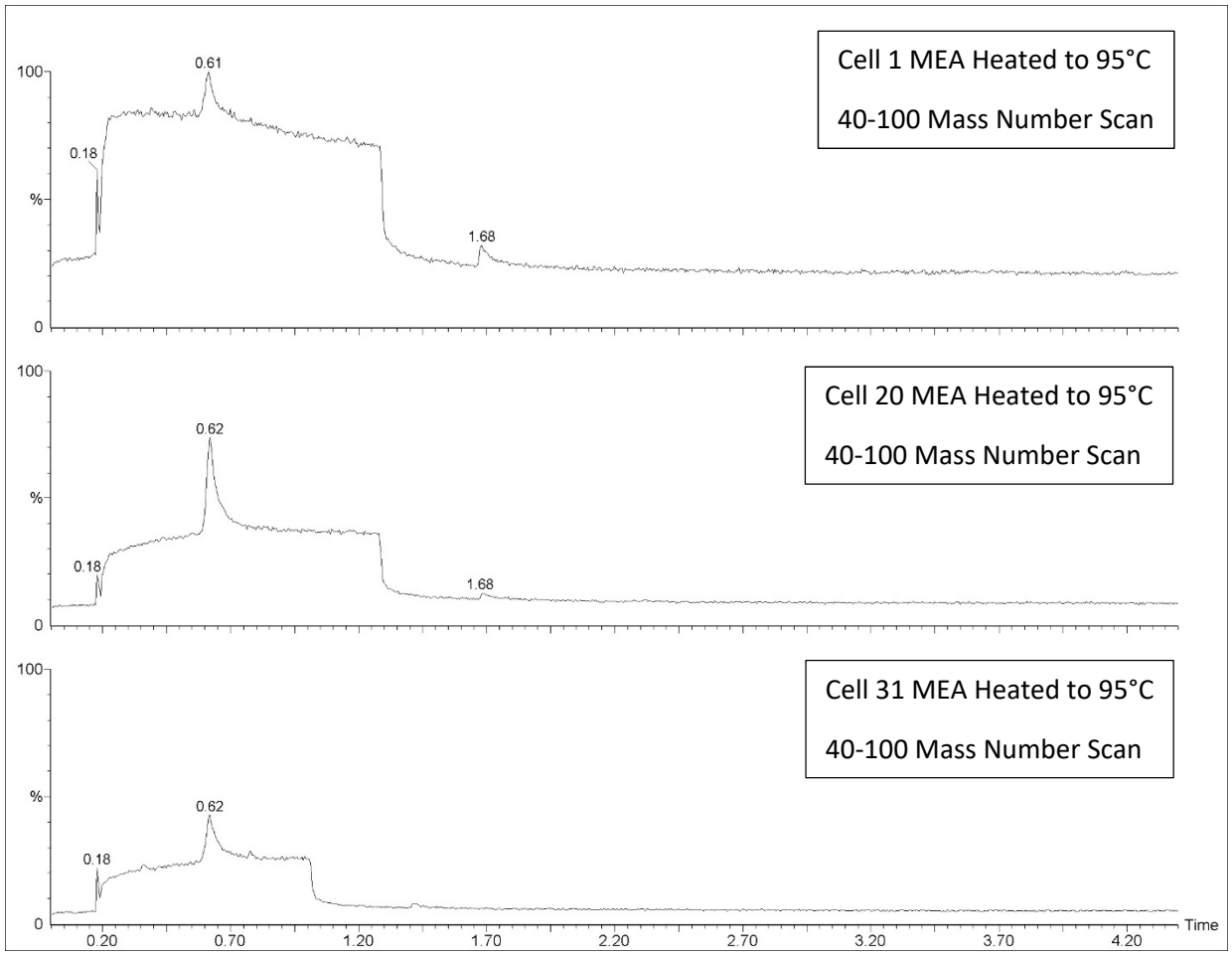

Figure 22: PEM Stack Membrane Electrode Assembly's (MEA) for Cell 1 (top), Cell 20 (middle) and Cell 31 (bottom) Heated to 95°C Chromatograms.

These results show a number of interesting trends. First, even without external heating, the MEA samples still have detectable levels of acetic acid that were eluted between 0.62-0.64min. This is most likely residual acetic acid from when the stack was being used, but also shows that there is a clear gradient in acetic acid concentrations with Cell 1 showing the largest concentration and Cell 31 having a very low acetic acid concentration. The acetic acid detected was all dissolved in the deionized water and no acetic acid as a separate phase was detected.

Next, when MEA samples were heated to 65°C, in Figure 21, the concentrations in all three MEA cells increased, when compared to the room temperature samples. The acetic acid concentrations (eluting between 0.64-0.65min) are much lower than what was observed from the FCATT PEM stack. Figure 10 shows that as the acetic acid concentration increases it starts to form as a separate phase at a later elution time. The increased number of MEA's in the PEM stack probably produced a larger quantity of acetic acid which formed acetic acid outside the deionized water. Only testing one MEA sample did not produce enough acetic acid for it to form as a separate phase. A clear gradient in acetic acid concentrations is still visible with Cell 1 showing the largest concentration and Cell 31 showing the lowest concentration. The acetic acid detected was all dissolved in the deionized water and no acetic acid as a separate phase was detected.

Finally, when MEA samples were heated to 95°C, in Figure 22, two events occurred. The first event is that the concentration of acetic acid dissolved in the deionized water decreased from when it was heated at 65°C. A hypothesis for a lower acetic acid concentration at 95°C is because only dilute acetic acid was produced. Concentrated acetic acid has a boiling point around 118°C, which is much greater than the 95°C boiling point for water, and should not evaporate to a large extent. In cases where acetic acid is very dilute its boiling temperature becomes close to that of water (100°C). This hypothesis can be verified through experimentation, which is demonstrated next.

Figure 23 shows the concentration change in a dilute acetic acid solution ($4.37 * 10^{-4}$ M) as it is heated at 95°C for several hours. The solution was initially tested before being heated at 95°C (bottom), tested after being heated for 4 hours at 95°C (middle) and tested after being heated for 6 ½ hours at 95°C (top). The small sample size should not change the acetic acid concentration significantly and only the evaporation process should change the concentration. The acetic acid peak (between 0.67 min and 0.71 min) dissolved in water gradually shrinks in area as the solution was allowed to heat for more and more time, until the peak was hardly noticeable.

The second event that occurred in Figure 22 is that acetic acid started to form as its own separate phase, which eluted at 1.68min. Up till now the only way to form acetic acid as a separate phase is by increasing the concentration of acetic acid dissolved in the water. Less acetic acid should be in the

deionized water due to it being evaporated, which would not make this possible. An explanation will be provided in Section 6 when the PEM stack electrocatalyst is discussed.

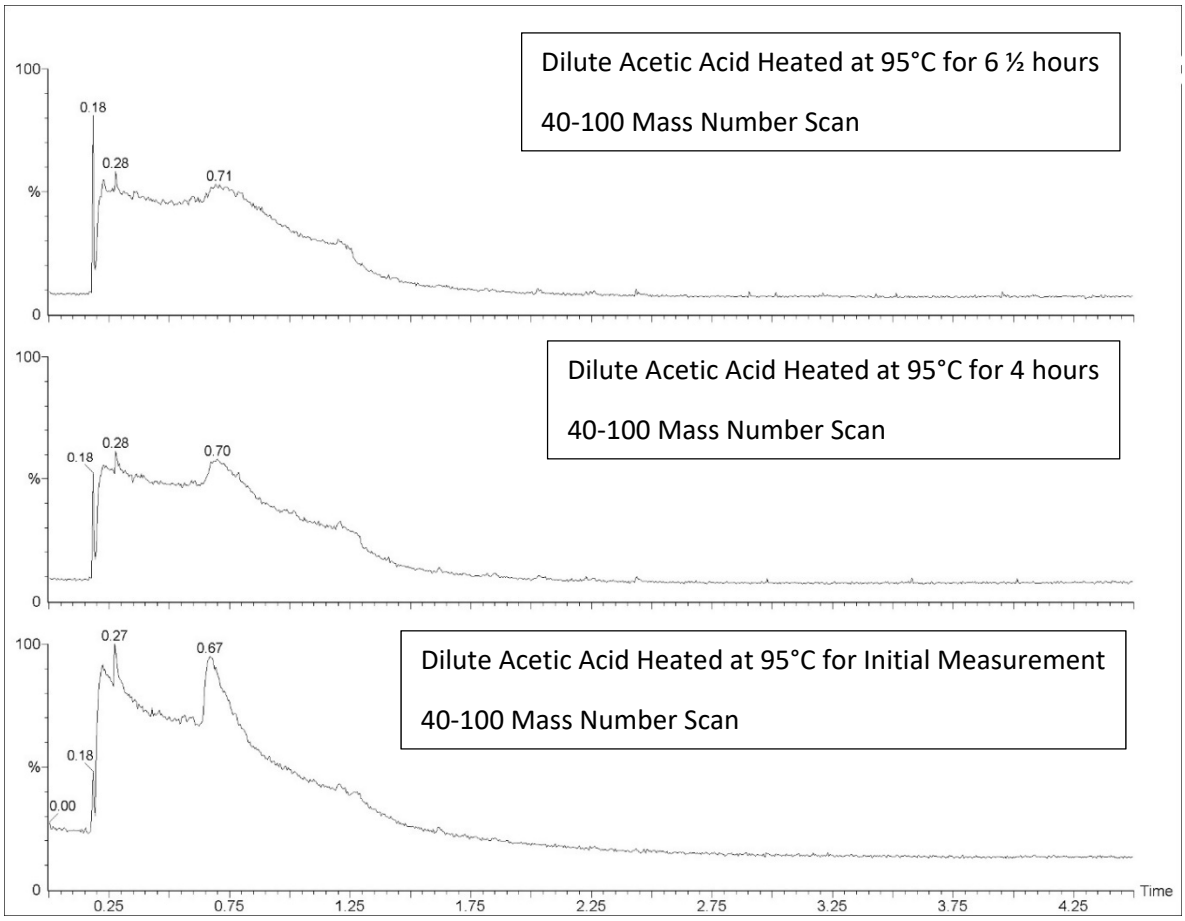

Figure 23: Dilute Acetic Acid Solutions Heated to 95°C for 6 ½ hrs (top), 4 hrs (middle), and the Initial Measurement (bottom) Chromatograms.

These results show that acetic acid was produced from the MEA at operating temperatures. Heat also was shown to play an important role in the increased production of the acetic acid from the MEA. No propionic acid was observed in these tests, compared to the FCATT exhaust water, but that may be due to a larger number of MEAs being present in the FCATT PEM stack, which would produce a larger concentration of propionic acid.

A list of the CAS # number(s) used to identify the compounds in the National Institute of Standards and Technology (NIST) database, where applicable, is shown below for the different samples.

5.2.1. Heated PEM Stack Membrane Electrode Assembly Water Compounds

Table 10 through Table 12 outlines the compounds found in the MS scan of the compounds found in Figure 20 through Figure 22. Table 13 outlines the compounds found in the MS scan of the compounds found in Figure 23. The location the compound originated at, such as in the sample or in the carrier gas, is listed in the "Origination" column.

Table 10: Heated PEM Stack Membrane Electrode Assembly Water Compounds from Figure 20

Compound Name	Mass Number (m/z)	Elution Time (min)	CAS #	Origination
PEM Stack Cell 1 Membrane Electrode Assembly at Room Temperature (21°C) (top)				
Acetic Acid in Water	60	0.62	64-19-7	Sample
PEM Stack Cell 20 Membrane Electrode Assembly at Room Temperature (21°C) (middle)				
Acetic Acid in Water	60	0.64	64-19-7	Sample
PEM Stack Cell 31 Membrane Electrode Assembly at Room Temperature (21°C) (bottom)				
Acetic Acid in Water	60	0.63	64-19-7	Sample

Table 11: Heated PEM Stack Membrane Electrode Assembly Water Compounds from Figure 21

Compound Name	Mass Number (m/z)	Elution Time (min)	CAS #	Origination
PEM Stack Cell 1 Membrane Electrode Assembly Heated at 65°C (top)				
Acetic Acid in Water	60	0.65	64-19-7	Sample
PEM Stack Cell 20 Membrane Electrode Assembly Heated at 65°C (middle)				
Acetic Acid in Water	60	0.64	64-19-7	Sample
PEM Stack Cell 31 Membrane Electrode Assembly Heated at 65°C (bottom)				
Acetic Acid in Water	60	0.64	64-19-7	Sample

Table 12: Heated PEM Stack Membrane Electrode Assembly Water Compounds from Figure 22

Compound Name	Mass Number (m/z)	Elution Time (min)	CAS #	Origination
PEM Stack Cell 1 Membrane Electrode Assembly Heated at 95°C (top)				
Acetic Acid in Water	60	0.61	64-19-7	Sample
Acetic Acid	60	1.68	64-19-7	Sample
PEM Stack Cell 20 Membrane Electrode Assembly Heated at 95°C (middle)				
Acetic Acid in Water	60	0.62	64-19-7	Sample
Acetic Acid	60	1.68	64-19-7	Samples
PEM Stack Cell 31 Membrane Electrode Assembly Heated at 95°C (bottom)				
Acetic Acid in Water	60	0.62	64-19-7	Sample

Table 13: Heated Dilute Acetic Acid Solution Compounds from Figure 23

Compound Name	Mass Number (m/z)	Elution Time (min)	CAS #	Origination
4.37 * 10^{-4} M Acetic Acid Heated to 95°C for 6 ½ hrs (top)				
Acetic Acid in Water	60	0.71	64-19-7	Sample
4.37 * 10^{-4} M Acetic Acid Heated to 95°C for 4 hrs (middle)				
Acetic Acid in Water	60	0.70	64-19-7	Sample
4.37 * 10^{-4} M Acetic Acid Heated to 95°C for the Initial Measurement (bottom)				
Acetic Acid in Water	60	0.67	64-19-7	Sample

The next section will show the results from heating the PEM material to temperatures close to the PEM stack operation temperature to narrow down if that is the component within the MEA that is degrading under applied heat.

5.3. Heated PEM Stack Proton Exchange Membrane

Figure 24 through Figure 26 show the water composition after heating PEM samples from Cells 1 (top), 20 (middle) and 31 (bottom) in deionized water for three 8-hr periods at: 1. room temperature (21°C) (Figure 24), 2. 65°C (Figure 25) and 3. 95°C (Figure 26). Acetic acid dissolved in the deionized water eluted between 0.61-0.65min but acetic acid did not form as a separate phase with any of the samples.

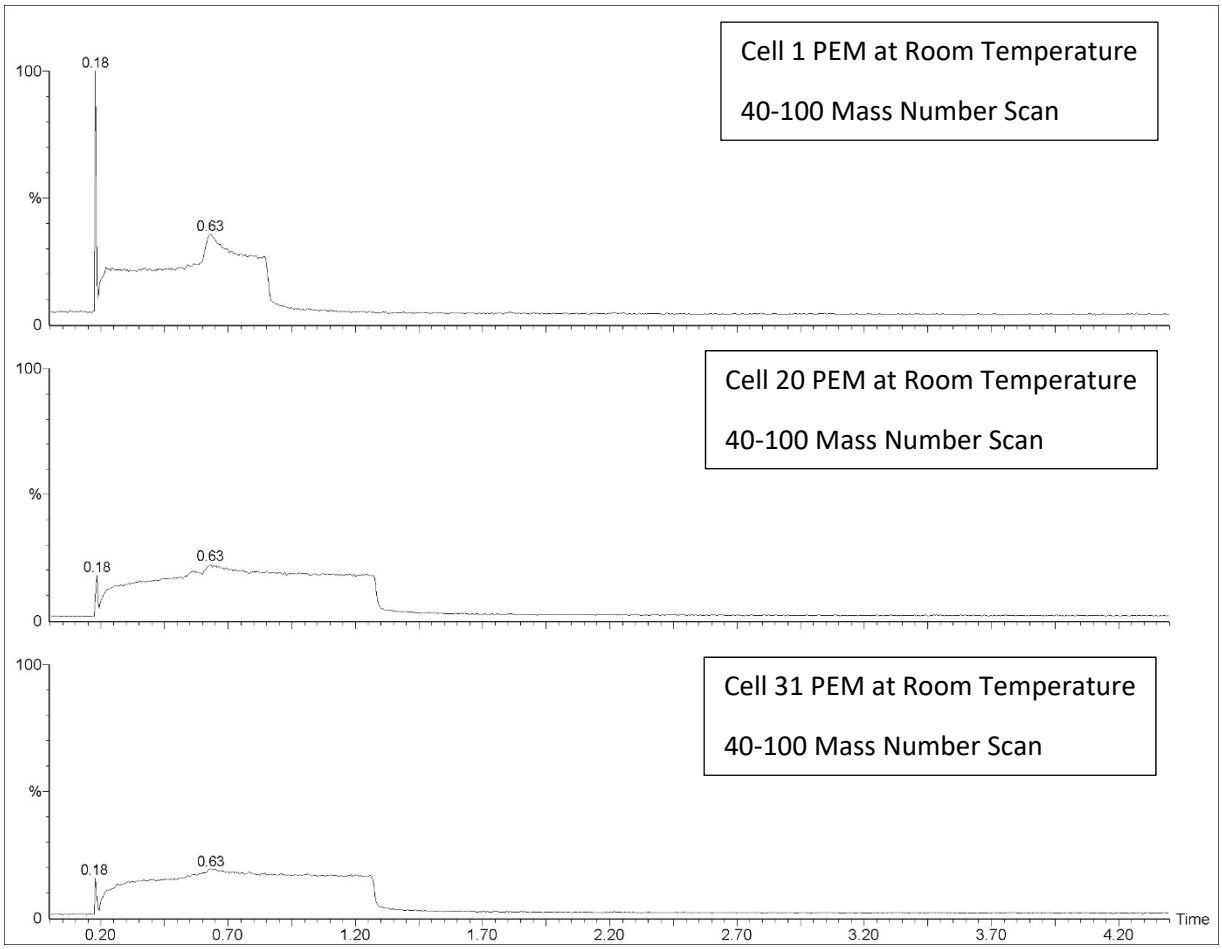

Figure 24: Proton Exchange Membrane (PEM) for Cell 1 (top), Cell 20 (middle) and Cell 31 (bottom) at Room Temperature Chromatograms.

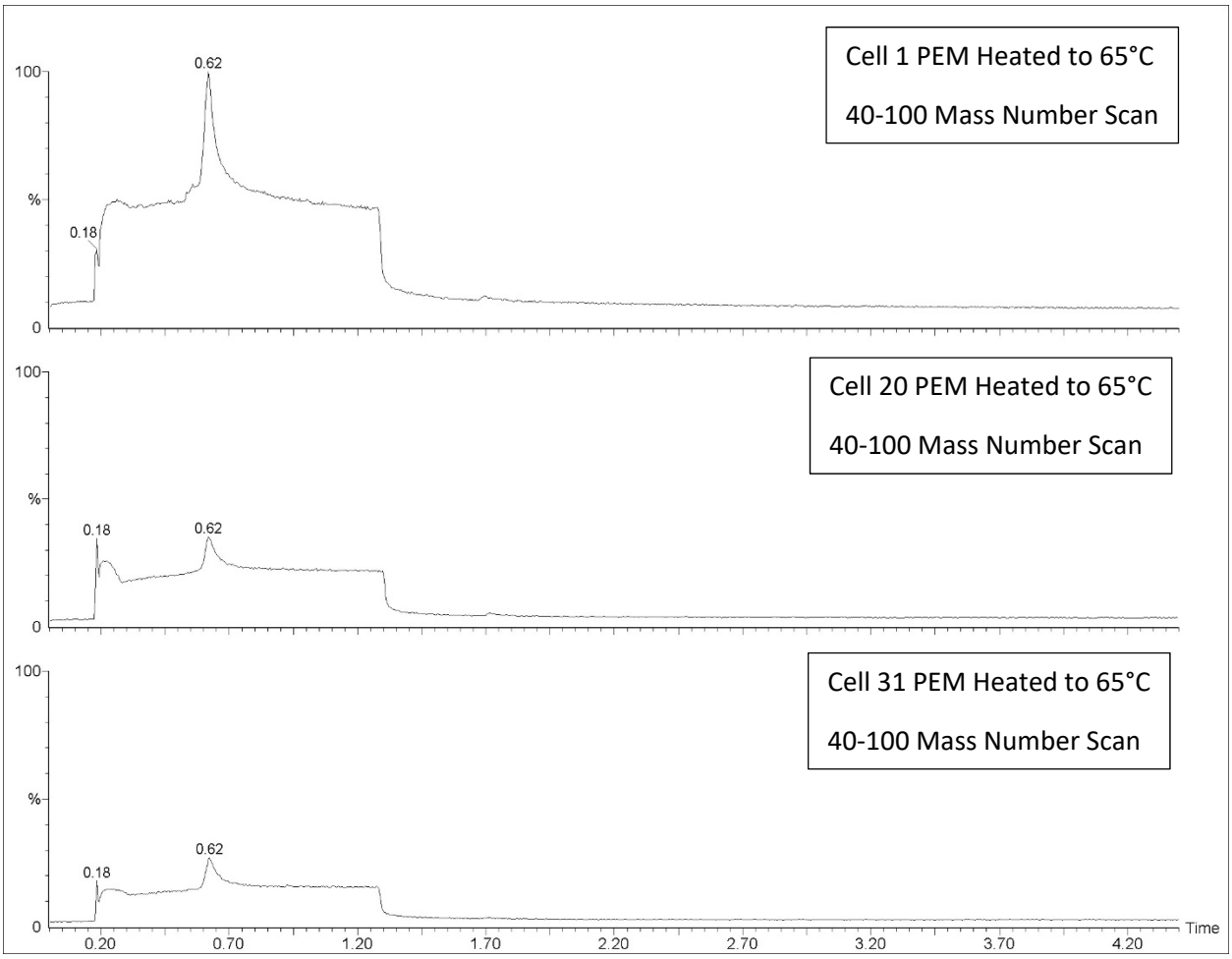

Figure 25: Proton Exchange Membrane (PEM) for Cell 1 (top), Cell 20 (middle) and Cell 31 (bottom) Heated to 65°C Chromatograms.

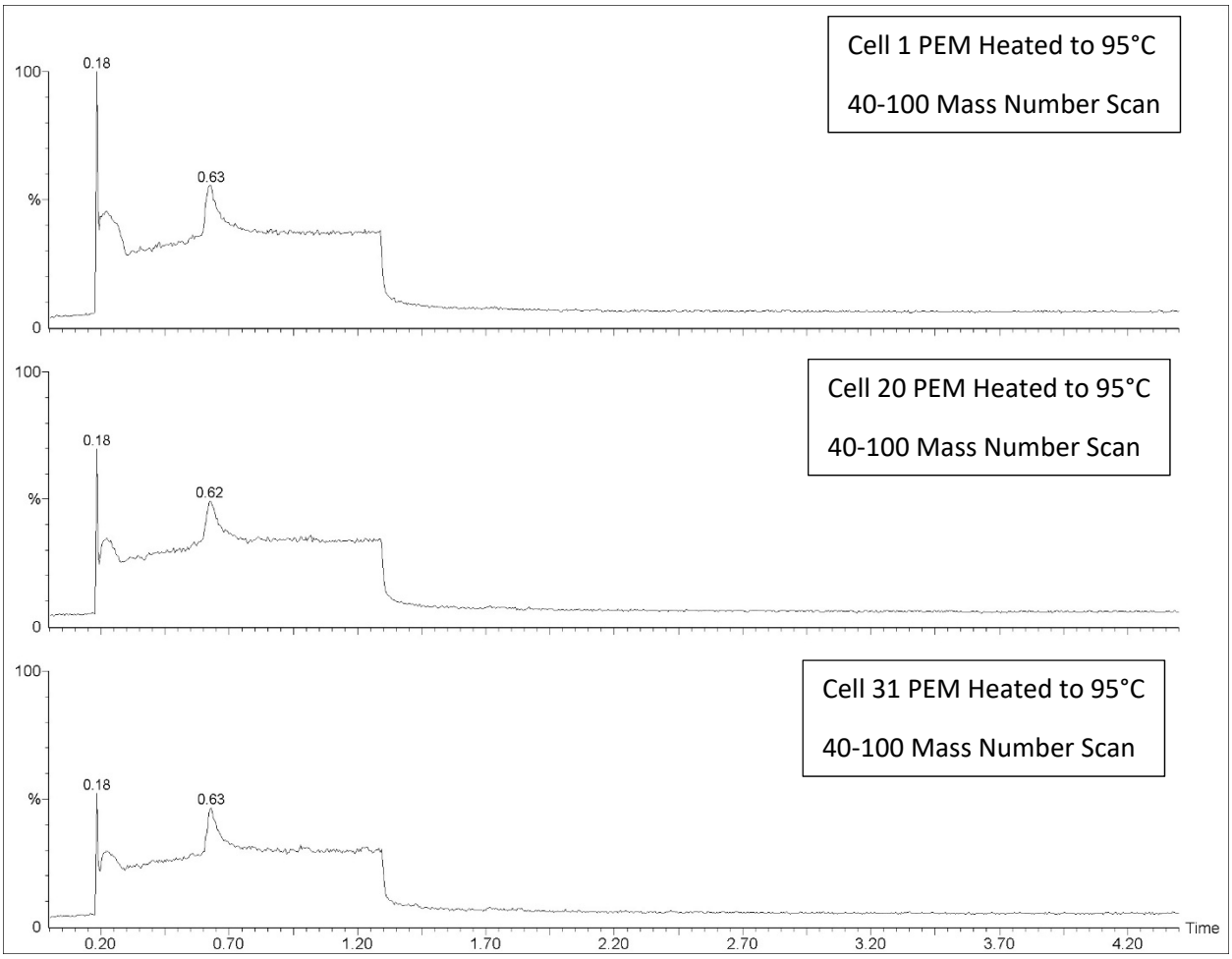

Figure 26: Proton Exchange Membrane (PEM) for Cell 1 (top), Cell 20 (middle) and Cell 31 (bottom) Heated to 95°C Chromatograms.

These results also show a number of interesting trends, compared to the results from the MEA samples. First, even at room temperature (Figure 24), the Cell 1 PEM sample had acetic acid being detected in noticeable quantities that were eluted at 0.63min. The Cell 20 and Cell 31 PEM samples had lower quantities of acetic acid detected being eluted at 0.63min. These trends match the data results from the MEA samples, where Cell 1 had the largest quantity of acetic acid compared to Cells 20 and 31. The acetic acid detected was all dissolved in the deionized water and no acetic acid as a separate phase was detected.

Next, when PEM samples were heated to 65°C, in Figure 25, the concentrations in all three PEM samples increased when compared to the room temperature samples, but Cell 1 still had the largest concentration of acetic acid. All three PEM samples eluted acetic acid dissolved in water at 0.62min and possibly a small peak at ~1.70min was present (which could be acetic acid as a separate phase), but acetic acid could not be identified.

Finally, when PEM samples were heated to 95°C, in Figure 26, the acetic acid concentrations in every sample were dramatically reduced to levels near the room temperature samples. This occurred for the same reason as the MEA samples heated to 95°C in that the acetic acid was evaporated away. The only other difference was that an addition peak did not appear around 1.68min as with the MEA samples.

5.3.1. Heated Proton Exchange Membrane and Dilute Acetic Acid Solution Compounds

Table 14 through Table 16 outlines the compounds found in the MS scan of the compounds found in Figure 24 through Figure 26. The location the compound originated at, such as in the sample or in the carrier gas, is listed in the "Origination" column.

Table 14: Heated Proton Exchange Membrane Water Compounds from Figure 24

Compound Name	Mass Number (m/z)	Elution Time (min)	CAS #	Origination
Cell 1 Proton Exchange Membrane at Room Temperature (21°C) (top)				
Acetic Acid in Water	60	0.63	64-19-7	Sample
Cell 20 Proton Exchange Membrane at Room Temperature (21°C) (middle)				
Acetic Acid in Water	60	0.63	64-19-7	Sample
Cell 31 Proton Exchange Membrane at Room Temperature (21°C) (bottom)				
Acetic Acid in Water	60	0.63	64-19-7	Sample

Table 15: Heated Proton Exchange Membrane Water Compounds from Figure 25

Compound Name	Mass Number (m/z)	Elution Time (min)	CAS #	Origination
Cell 1 Proton Exchange Membrane Heated to 65°C (top)				
Acetic Acid in Water	60	0.62	64-19-7	Sample
Cell 20 Proton Exchange Membrane Heated to 65°C (middle)				
Acetic Acid in Water	60	0.62	64-19-7	Sample
Cell 31 Proton Exchange Membrane Heated to 65°C (bottom)				
Acetic Acid in Water	60	0.62	64-19-7	Sample

Table 16: Heated Proton Exchange Membrane Water Compounds from Figure 26

Compound Name	Mass Number (m/z)	Elution Time (min)	CAS #	Origination
Cell 1 Proton Exchange Membrane Heated to 95°C (top)				
Acetic Acid in Water	60	0.63	64-19-7	Sample
Cell 20 Proton Exchange Membrane Heated to 95°C (middle)				
Acetic Acid in Water	60	0.62	64-19-7	Sample
Cell 31 Proton Exchange Membrane Heated to 95°C (bottom)				
Acetic Acid in Water	60	0.63	64-19-7	Sample

The results shown thus far have shown the following general trends: 1. The PEM material in the MEA located in the PEM stack was the cause of the acetic acid being produced in the FCATT exhaust water, 2. The Cell 1 PEM material, which is closest to the stack manifold, was producing the largest amount of acetic acid and 3. Higher operating temperatures resulted in acetic acid forming as a separate phase outside the deionized water. One hypothesis why the PEM material in Cell 1 had degraded more than the other cells, which was previously alluded to in Section 4, was that the manifold and attached balance of plant components may be acting as a heat sink which lowered the operating temperature of Cell 1. A lower cell temperature would lower the cell voltage [3, 4] which increases its overall overpotential by increasing its ohmic losses in the cell. The increased overtpotential indicate Cell 1 is not as efficient and those energy losses are transformed into increased heat within the cell and degrade the PEM material further.

A second item of note was that the recorded temperature of the cooling fluid, for the data presented in Figure 17 and Figure 18 was between 71°C and 75°C, which is noticeably higher than the manufacturer's maximum operating temperature of 65°C. The cooling fluid set-point was increased for FCATT PEM fuel cell since the recommended cooling temperature set-point was difficult to achieve. Based on how sensitive the PEM material degradation was to changes in operating temperature this increase in cooling temperature may have resulted in increased degradation over the entire stack as well.

The remaining sections will only show data from Cell 1 and 31 since they demonstrate the clearest difference between the most degraded (Cell 1) and least degraded (Cell 31) MEA's in the stack. The next sections will investigate the structural, physical, and elemental properties of the electrolyte material to help understand the cause of the thermal degradation.

5.4. PEM Stack Proton Exchange Membrane Energy Dispersive Spectroscopy Characterization

The PEM material in Cell 1 and Cell 31 were analyzed using Energy Dispersive Spectroscopy (EDS) (located at TARDEC in building 200C in the Metallurgy laboratory) to determine their elemental compositions, which were important to help determine the cause of thermal degradation. In addition, any differences in elemental compositions between the two cells could prove useful in identification of failure modes.

Figure 27 shows the EDS scan of the baseplate used to hold the PEM material samples. The elemental composition was carbon (0.277 keV), oxygen (0.525 keV), sodium (1.04 keV), magnesium (1.25 keV), aluminum (1.48 keV), silicon (1.73 keV), gold (2.12 keV, 9.71 keV) and chlorine (2.62 keV). The baseplate was primarily composed of aluminum. All other elements were from the sputtering process or from trace organic matter on the baseplate.

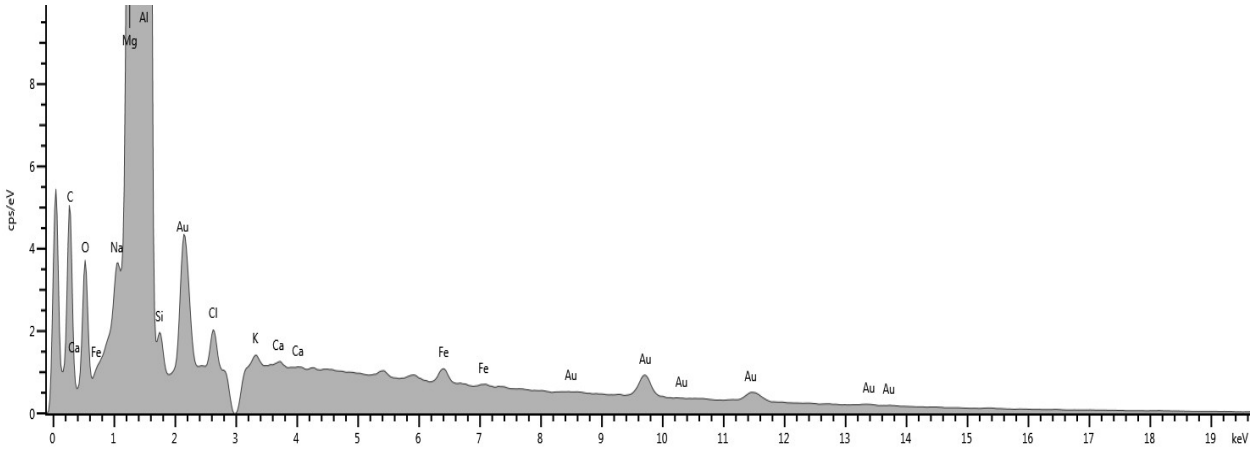

Figure 27: Sample Baseplate Energy Dispersive Spectroscopy Scan Results

Figure 28 shows the EDS scans the of PEM material from Cell 1 (left) and Cell 31 (right). The elemental composition from both sample scans were primarily carbon (0.277 keV), oxygen (0.525 keV), aluminum (1.48 keV), silicon (1.73 keV), copper (8.04 keV) and gold (2.12 keV, 9.71 keV). The aluminum peak and possibly some of the silicon peak are from the baseplate, the gold peaks are from the gold that was sputtered onto the sample and the copper peaks are from the copper tape used to hold the samples in place on the baseplate. If both the silicon and aluminum peak height ratios in Figure 28 originated from the baseplate then the aluminum peak would be greater than the silicon peak, but it is substantially smaller, which indicates the presence of silicon in Cells 1 and 31.

Overall the PEM material from Cells 1 and 31 were composed of carbon, oxygen, and silicon. Typical PEM materials used in MEA construction include: 1. Sulfonated perfluorinated polymers (such as Nafion [5, 6, 7, 8]); 2. CsH_2PO_4 [8]; 3. Phosphotungstic acid (PWA) [8]; 4. Polybenzimidazole (PBI) [8, 9]; 5. $CsHSO_4$ [8]; 6. H_3PO_4 [8]; and 7. $Zr(HPO_4)_2H_2O$ [8]. Comparison of the results in Figure 28 to these possible different materials shows that the Sulfonated perfluorinated polymers, CsH_2PO_4, PWA, $CsHSO_4$, H_3PO_4, and $Zr(HPO_4)_2H_2O$ materials can be eliminated as possibilities because sulfur, cesium, phosphorous, and zirconium were not present in detectable levels in Figure 28, and would have been detectable if present.

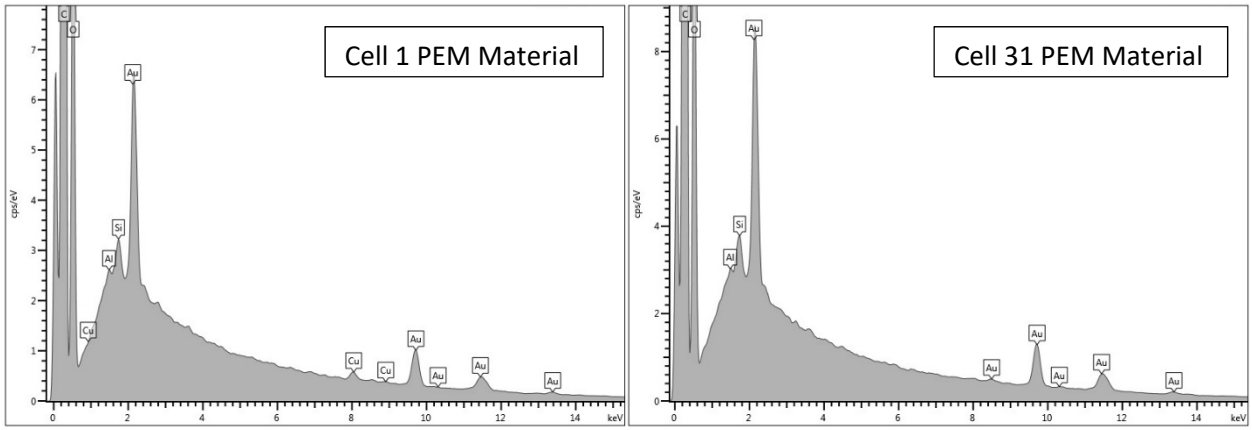

Figure 28: PEM Stack Proton Exchange Membrane Cell 1 (left) and Cell 31 (right) Energy Dispersive Spectroscopy Scan Results.

The only material not eliminated was PBI, which is made of carbon, nitrogen and hydrogen. While nitrogen was not detected in Figure 28 it still may be overshadowed by the background noise. Literature studies [10] have shown that PBI can be doped with silicon nanoparticles to increase both the mechanical strength and thermal stability of the polymer, which may be the cause of silicon being identified. The presence of oxygen in the sample is also likely associated with the silicon in the form of silicon dioxide. Additional characterization of the PEM material will be necessary to confirm whether silicon dioxide doped PBI is being used.

The next section will characterize the structural properties of the PEM material using Fourier-Transform Infrared (FTIR) Spectroscopy to help identify the compound structure further.

5.5. PEM Stack Proton Exchange Membrane Fourier-Transform Infrared Spectroscopy Characterization

The PEM material in Cell 1 and Cell 31 were analyzed using FTIR (located at TARDEC in building 215 in the Elastomer, Isomer, Polymer laboratory) to help determine what compounds the material was made

from. The elemental composition between the two samples may be the same, but the chemical structure may have been altered from thermal degradation.

Figure 29 and Figure 30 show the FTIR results of Cell 1 and Cell 31, respectively. Both samples had peak locations at similar wavenumbers, but just with different absorbance amounts. Cell 1 typically has higher absorbance values, than Cell 31, at wavelengths between 4,000 and 2,700 cm^{-1}, while having lower absorbance values from 2,000 and 500 cm^{-1}. These changes in absorbance between Cell 1 and Cell 31 provide additional evidence that structural changes have occurred between the two cells.

Analysis of the two samples using the FTIR chemical compound database yielded a 36.47% match with Trimer Acid and a 34.13% match with Polyvinyl Ester, which did not provide an adequate level of accuracy to make any conclusions.

Cell 1 and 31 FTIR results were compared to PBI FTIR results reported in various literature studies [10, 11, 12, 13, 14]. Peaks located at 1612.33 cm^{-1}, 1270.00 cm^{-1}, 1462.50 cm^{-1}, 1180.00 cm^{-1}, 829.09 cm^{-1} and 800.83 cm^{-1} could be matched to some [12, 14] but not all the mentioned literature results. Even within the reported pure PBI results (no other compounds were added to the PBI) found in literature there was a significant difference in peak locations. Since there was such a deviation between reported pure PBI FTIR results, and the fact that a number of peaks were matched, it is realistically possible that PBI was used in the manufacture of the PEM material. Differences in peak locations could also possibly be attributed to additives that were included in the formulation of the PEM material. Different fabrication techniques could also impact the structure of the PEM material making comparison to the literature imprecise. Additional characterization techniques will need to be used to improve identification of the PEM material.

Although identification of the PEM material could not be achieved, verification of silicon in the sample was found through literature sources. Literature [10, 15, 16] has shown that the 3300.17 cm^{-1} and 2922.00 cm^{-1} peaks are related to silicon located in the sample. The 3300.17 cm^{-1} peak was specifically identified as silicon bonded to the OH group from water.

The characterization results shown thus far further suggest that the PEM material used was PBI that was doped with silicon dioxide. The following section will further characterize the structural properties of the PEM material using XRD and compare those results to XRD scans reported in literature. In addition to material identification, XRD will be used to study the effects heat have on the structural properties of the PEM material.

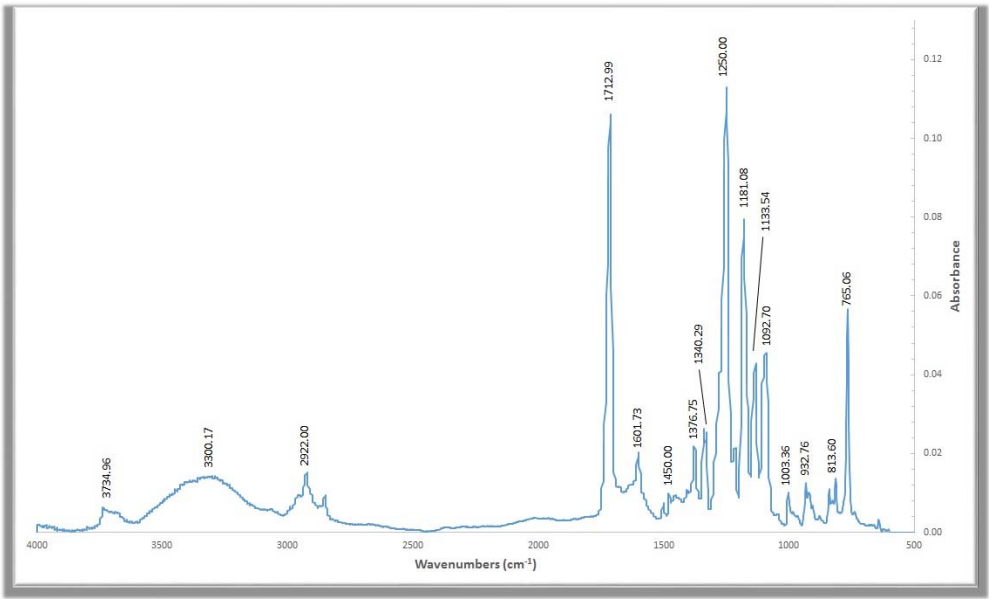

Figure 29: PEM Stack Proton Exchange Membrane Cell 1 Fourier-Transform Infrared Spectroscopy Scan Results.

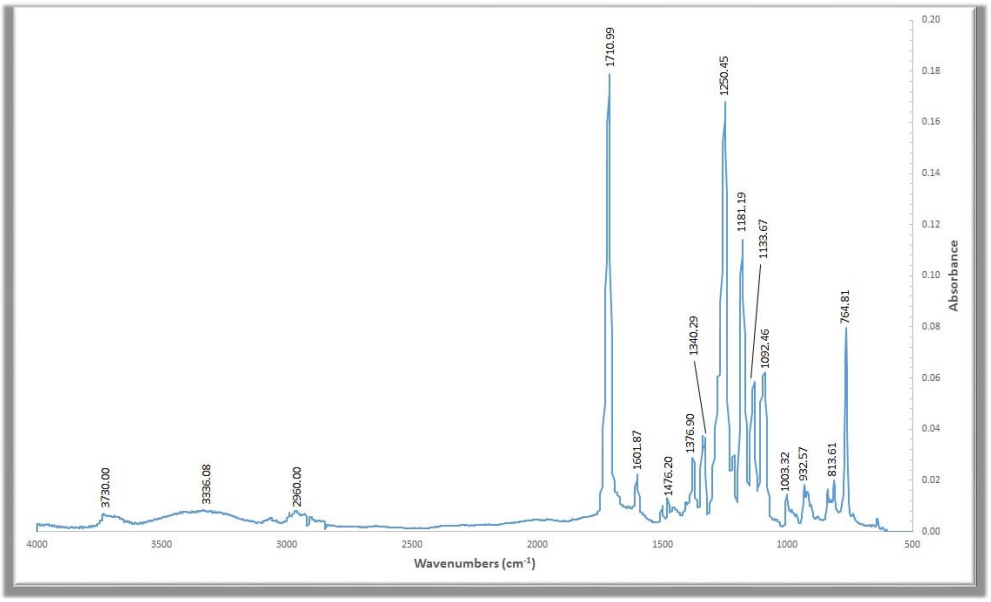

Figure 30: PEM Stack Proton Exchange Membrane Cell 31 Fourier-Transform Infrared Spectroscopy Scan Results.

5.6. PEM Stack Proton Exchange Membrane X-Ray Diffraction Characterization

The PEM samples (from Cell 1 and 31) that were previously heated at various temperatures in deionized water (and then had the water characterized with the GC/MS) were then characterized using XRD (located at TARDEC in building 200C in the Metallurgy laboratory).

Figure 31 shows the XRD data for Cell 1 (plots A and B) and Cell 31 (plots C and D) for the unheated (21°C), 65°C, and 95°C PEM samples. Each XRD scan was conducted between 10-90° 2θ to determine if changes in d-spacing, particle size or if material phase changes occurred. Plots A and C show the entire scan and plots B and D show a more detailed view of the main peak for improved resolution.

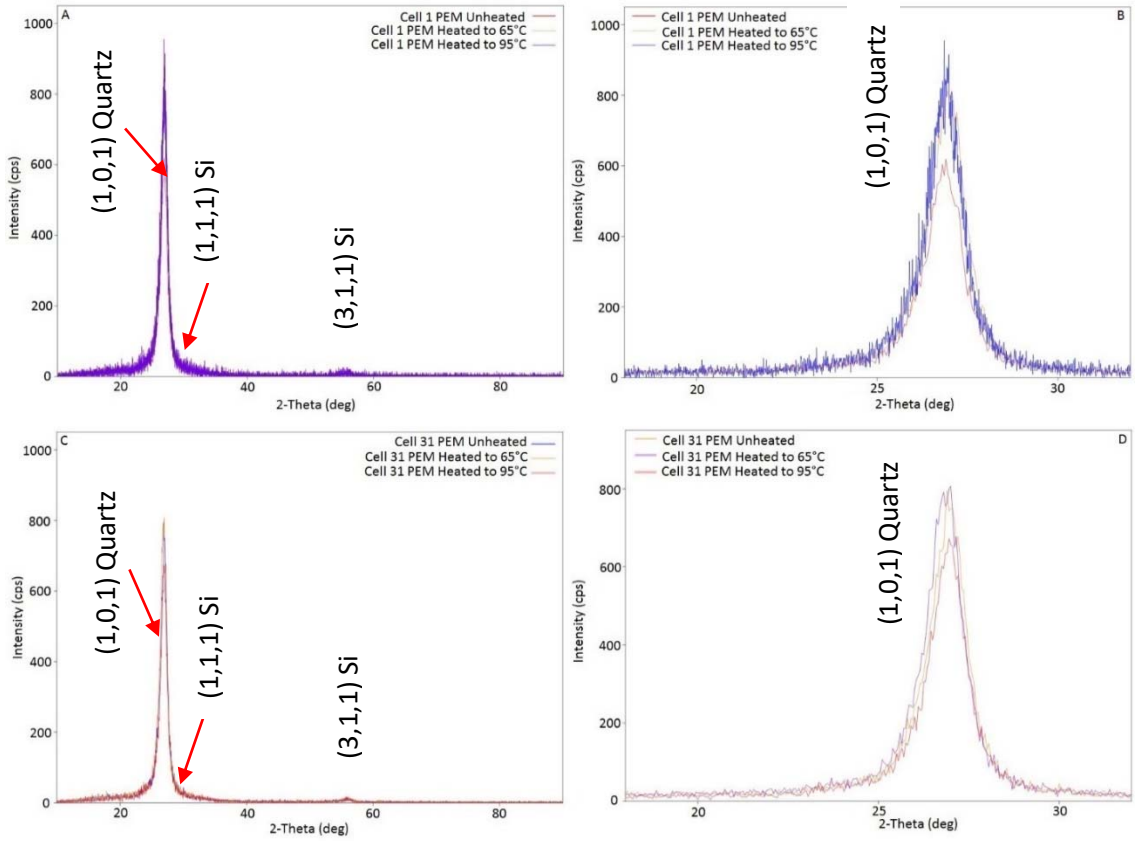

Figure 31: PEM Stack Proton Exchange Membrane (PEM) XRD Data from 10-90° 2θ. PEM Samples were from Cell 1 (plots A and B) and Cell 31 (plots C and D). Samples from Cell 1 and 31 were Heated to 95°C, 65°C and Unheated (21°C).

Cells 1 and 31 show two peaks. Both cell have the peak locations with the main peak at 26.9° 2θ and the smaller peak at 55.9° 2θ. Initially this shows that the increased PEM material degradation in Cell 1 did not change the d-spacing enough for the XRD to detect. In addition these results show that the degradation seen in Cell 1 has not promoted material phase changes compared to Cell 31. The effect of increasing temperature, within a specific cell, did not appear to have any noticeable impact on the crystallinity (peak height). The material may be thermally stable enough to not change under this level of degradation or both Cell 1 and 31 could have already been degraded beyond the point where thermal degradation will increase crystallinity.

Figure 32 compares XRD scans of Cell 1 against literature studies [10, 17] for PBI with and without silicon dioxide added. Since Cell 1 and 31 were shown to have the exact peak location only Cell 1 will be used for simplicity. The intensity of each data set has been adjusted to make all the data fit onto the same scale, so intensity comparisons between the data sets should not be made, only a comparison between the peak locations on the x-axis. The data presented in the literature shows the following information: 1. Pure PBI has its main peak at ~22.7° 2θ and 2. The addition of silicon dioxide shifts the main peak to a higher 2θ value. The collected XRD data from Cells 1 and 31 was located at an even greater 2θ value, which implies, coupled with the previously shown EDS and FTIR results, that silicon dioxide was added to PBI and used as the PEM material. The collected data from Cells 1 and 31 also show a much sharper peak compared to the literature data which suggests the PEM material had more crystallinity.

Figure 33 shows the same data as Figure 32 except the intensity data was not scaled to fit onto the same y-axis scale. The Cell 31 XRD data has a much sharper and taller peak than the literature data, which shows the addition of silicon dioxide made the PEM material more structured and ordered, which increased its crystallinity compared to the pure PBI reported in the literature.

There are many different structures that silicon dioxide could take which all have different crystallinity. Literature [18] results show that the structure of the silicon dioxide appears to be quartz with a very sharp intense main peak at 26.6° 2θ, which is very close to the 26.9° 2θ value found in both Cell 1 and 31. Closer analysis using the Rigaku material database confirmed that Quartz did have its main peak located at 26.9° 2θ (database # 1532512). Analysis of the second, smaller peak at 55.9° 2θ, showed it to be the element silicon (database #4507226), which was what remained from the formation of quartz.

The addition of quartz to the PEM material as particles should be visible through EDS elemental mapping, which would also provide concrete proof of the quartz existence and also useful information on the particle size and particle distribution throughout the PEM material.

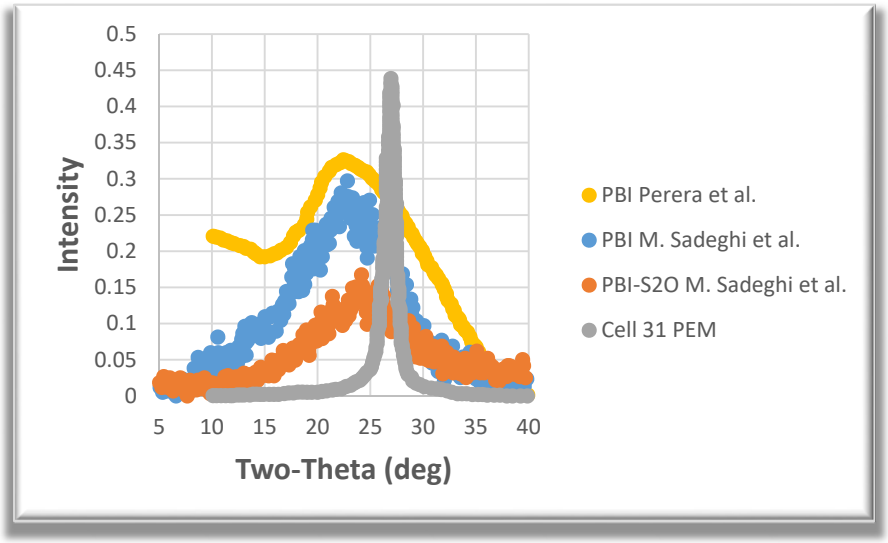

Figure 32: XRD Scan Comparison for Cell 31 and PBI Literature Studies. Intensity Data is Scaled for Easier Comparison of Peak Position.

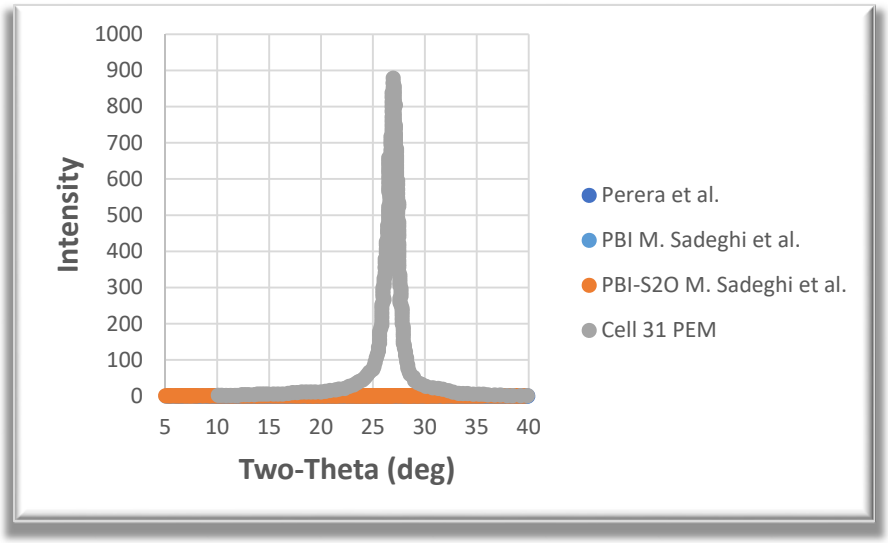

Figure 33: XRD Scan Comparison for Cell 31 and PBI Literature Studies. Intensity Data is not Scaled.

5.7. PEM Stack Proton Exchange Membrane Scanning Electron Microscopy Elemental Mapping Characterization

The following information will show elemental mapping superimposed on top of SEM images to determine if particles found in the PEM material are quartz or have other elemental compositions.

Figure 34 shows an SEM image and elemental mapping of the Cell 1 PEM material taken at 300x magnification. The elements of carbon (red), oxygen (light green), silicon (magenta) and aluminum (teal) were mapped and superimposed on top of the SEM image. The silicon was mapped because the presence of SiO_2 was being investigated, and the other elements were mapped because they are prominent in the EDS scan shown earlier.

Figure 35 shows SEM images and elemental mappings of the Cell 31 PEM material taken at 150x magnification and 1,000x magnification (which is an area from the first image). The same elements as with Cell 1 were mapped, for the same reasons listed before.

Both figures show that silicon and oxygen are present in particles located through the PEM material, but aluminum is also present to some degree in those same particles. Aluminum was originally thought to be present in the EDS scans since the baseplate was made of aluminum metal, but these results indicate aluminum was also doped into the PEM material to possibly increase the PEM material thermal stability. Another observation is that the oxygen, silicon and aluminum are detected at much lower magnifications in Cell 1 than in Cell 31. Very large silicon and aluminum deposits are detected in Cell 1 at 300x, but Cell 31 does not show nearly any silicon or aluminum deposits at 150x magnification. An increase in magnification to 1,000x was required in Cell 31 to detect any appreciable amounts of silicon or aluminum. This indicates that these elements are agglomerating and/or segregating into larger particles under increased degradation, which Cell 1 has clearly shown. The smallest particle size that could be detected outside of the background noise the SEM and EDS was 500nm. As Sadeghi et al [10] had used SiO_2 particles 147nm or smaller, it is possible that silicon and aluminum particles were added that were smaller than what the SEM and EDS could detect, and have agglomerated/segregated as the amount of degradation was increased.

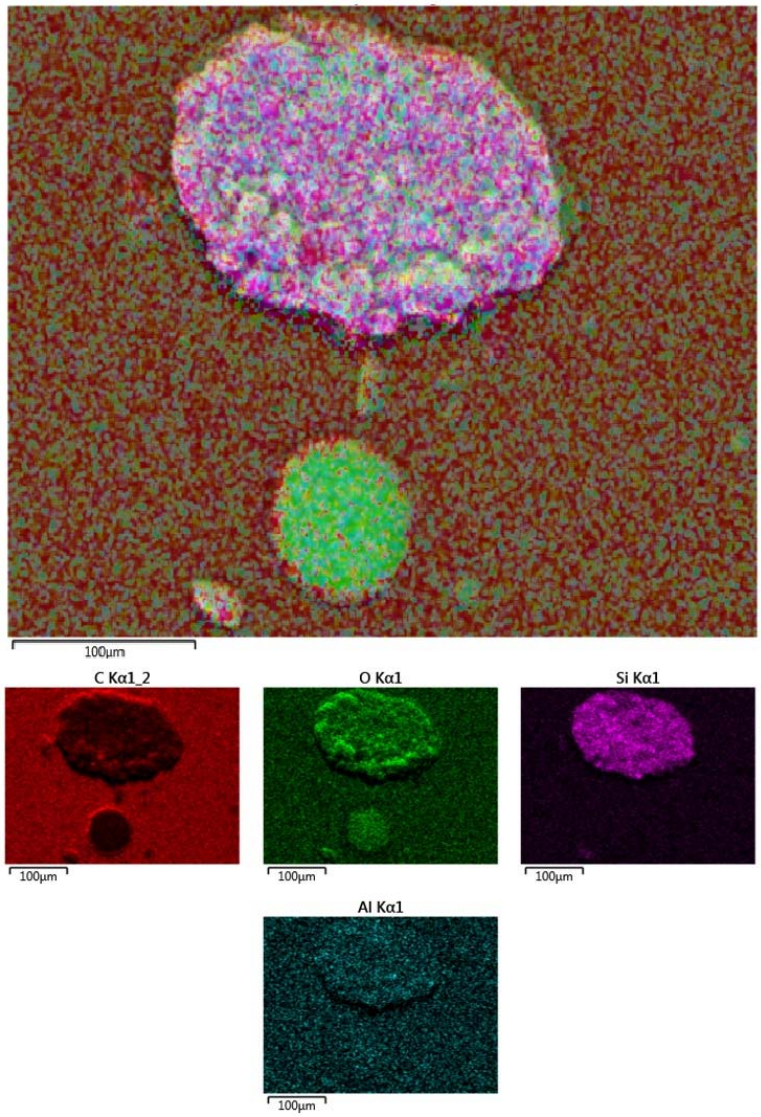

Figure 34: Cell 1 PEM Material SEM Image and EDS Elemental Mapping at 300x Magnification. Carbon (red), Oxygen (light green), Silicon (magenta), and Aluminum (teal) Elements are Super-Imposed on the Original SEM Image.

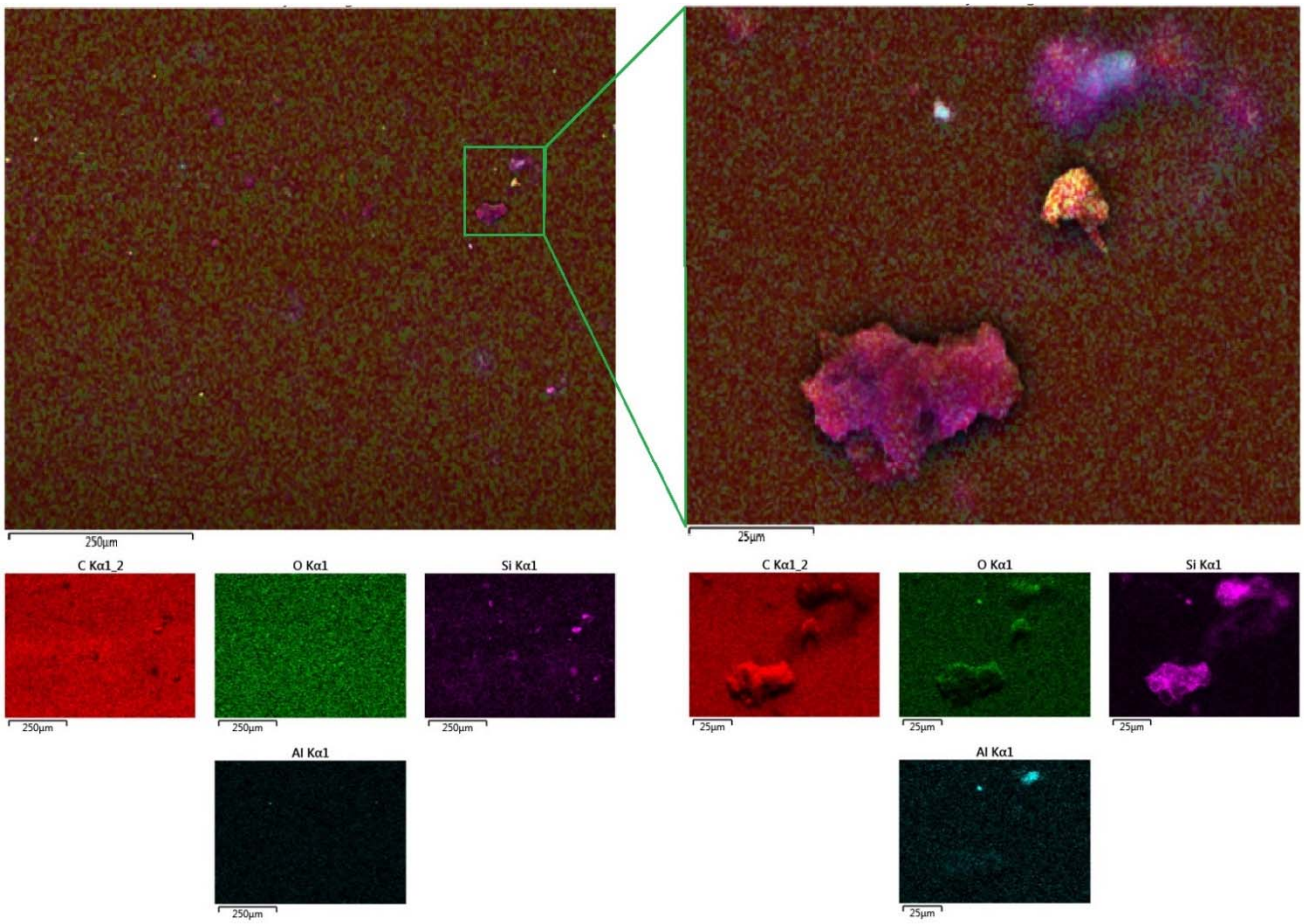

Figure 35: Cell 31 PEM Material SEM Image and EDS Elemental Mapping at 150x Magnification (left). A Section of the Left Image is Shown at 1,000x Magnification (right). Carbon (red), Oxygen (light green), Silicon (magenta), and Aluminum (teal) Elements are Super-Imposed on the Original SEM Image.

The final section that characterizes the PEM material will investigate the impact that the addition of silicon and aluminum had on the decomposition temperature of the PEM material and compare those results to the published decomposition temperature for PBI.

5.8. PEM Stack Proton Exchange Membrane Thermo-Gravimetric Characterization

Both Cells 1 and 31 were characterized using Thermo-Gravimetric Analysis (TGA) to determine the following: 1. Did increased degradation affect the thermal decomposition profile? and 2. How much was the thermal stability of the PEM material increased when compared to PBI literature sources?

Figure 36 shows the recorded TGA decomposition data from Cells 1 and 31, taken from 30-700°C using a nitrogen atmosphere, compared to literature sources of PBI TGA data [17, 19, 20].

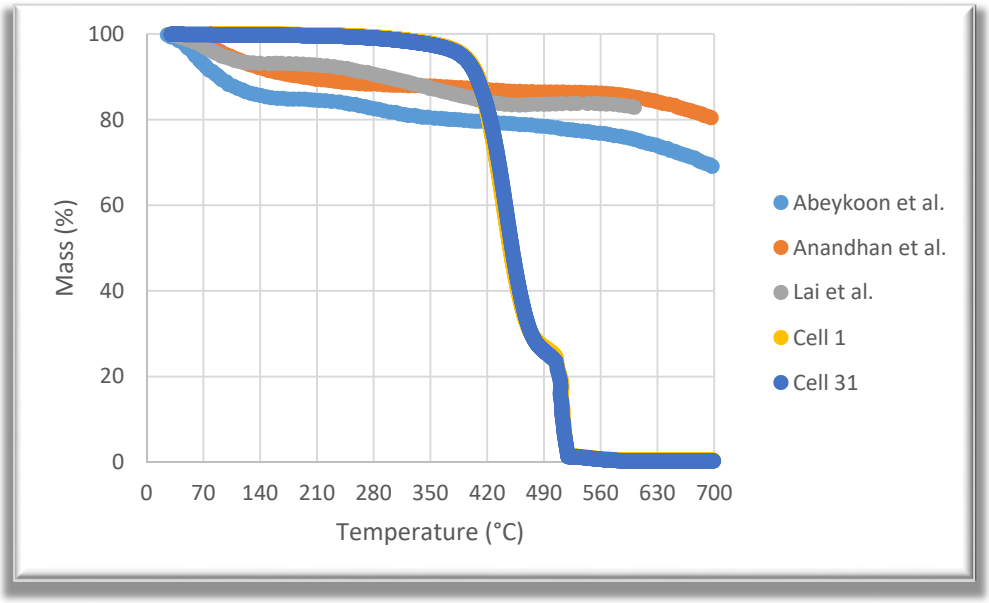

Figure 36: TGA Curve Comparison for Cell 1, Cell 31 and PBI Literature Studies between 30°C and 700°C.

An initial glance using a high level view shows that Cells 1 and 31 show an increased thermal stability, compared to the PBI literature sources, starting around 90°C until Cells 1 and 31 start to heavily degrade around 410°C. At temperatures above 420°C the PBI literatures sources maintain a significantly higher thermal stability up to 700°C, where they start to show a decrease in mass. Since the FCATT PEM stack did not operate at these elevated temperatures a second TGA plot will show the TGA plots between 30-300°C, which is realistic temperature range for the FCATT PEM stack to operate within.

Figure 37 shows an enlarged region of the data presented in Figure 36 from 30-300°C. This enlarged region shows that Cells 1 and 31 are almost identical in their decomposition temperature even at lower

operating temperatures, so degradation does not seem to impact the thermal decomposition noticeably. The addition of silicon and aluminum to the PBI appears to significantly increase the thermal stability. Both Cells 1 and 31 take nearly an additional 250°C to reach the same mass loss as the pure PBI, when starting at 65°C.

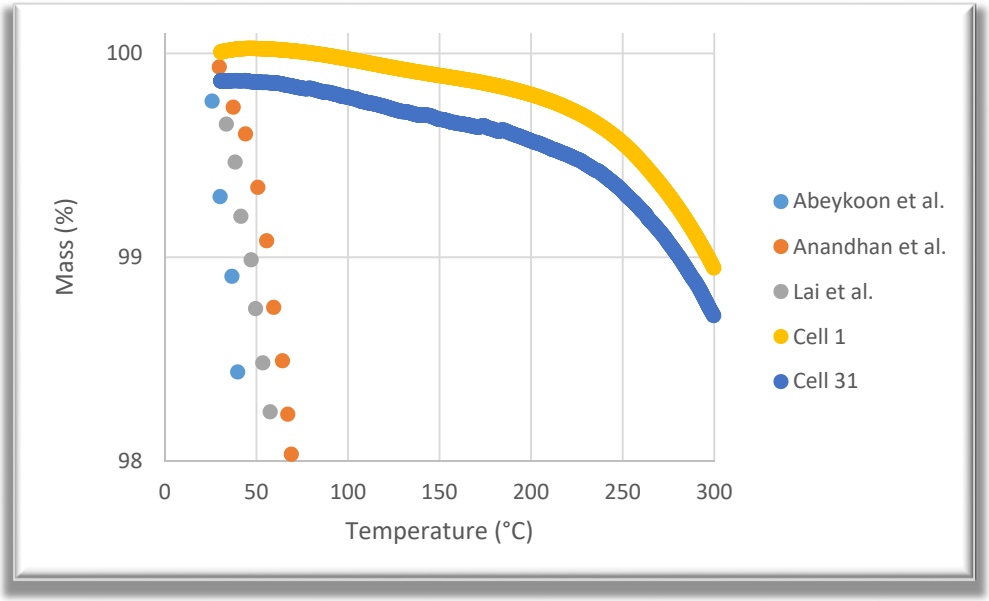

Figure 37: TGA Curve Comparison for Cell 1, Cell 31 and PBI Literature Studies between 30°C and 300°C.

Even though there is a significant reduction in mass loss between Cells 1/31 and PBI from literature there does still exist a mass loss of 0.4% between 30-200°C, which could still contribute to further degradation of the stack.

The following section will characterize the electrocatalyst and try to identify what material was used and whether it contributed to the acetic acid formation.

5.9. Membrane Exchange Assembly and Proton Exchange Membrane Characterization Summary

Characterization of the MEA and PEM material showed the following information:

1. The PEM material in both Cell 1 and 31 was being degraded, which promoted the formation of acetic acid in the water. The PEM material was degraded through applied external heat and temperatures 65°C or greater showed noticeable levels of acetic acid produced. Cell 1 produced a greater amount of acetic acid, compared to Cell 31, most likely due to its increased degradation. The exact mechanism for the acetic acid production is unknown at this time.
2. The operating temperature of the FCATT PEM stack was 6°C to 10°C above the manufacturer's recommended maximum operating temperature, which may have resulted in the entire stack degrading at an elevated rate.
3. Characterization of the Cell 1 and 31 PEM material using EDS, FTIR and XRD showed both samples to be likely composed of PBI. The PEM material was doped with quartz (SiO_2), aluminum and possibly other additives.
4. Characterization of the Cell 1 and 31 PEM material using SEM and EDS elemental mapping showed particles that contained silicon, oxygen and aluminum. The silicon and aluminum particle sizes in Cell 1 showed were larger in size than Cell 31, possibly due to increased agglomeration from increased degradation.
5. The XRD scans for Cells 1 and 31 were nearly identical in peak position and intensity. The increased thermal degradation of Cell 1 did not noticeably impact these results.
6. Characterization of the Cell 1 and 13 PEM material using TGA showed increased thermal resistance compared to the PBI material. An additional 250°C of heating was required, when starting at an operating temperature of 65°C, for Cells 1 and 31 to reach the same mass loss in their respective PEM material as PBI TGA results shown in literature.
7. The TGA curves for Cells 1 and 31 were nearly identical and the increased thermal degradation of Cell 1 did not affect its thermal decomposition profile significantly.

6. Impact Electrocatalyst has on Acetic Acid Formation and Electrocatalyst Characterization

6.1. Introduction

The previous section determined the root cause of the acetic acid production was due to the Cell PEM material (primarily from Cell 1) thermally decomposing at temperature 65°C or greater. Acetic acid produced from the thermal decomposition experiments of the PEM material was found dissolved in the water, while exhaust water collected from the FCATT PEM stack contained acetic acid that had formed as a separate phase outside the water. This section will investigate the electrocatalyst material used in the MEA to determine whether it contributed to acetic acid forming its own phase

6.2. Electrocatalyst Elemental Composition Analysis

The electrocatalyst material, from both the cathode and anode sides, of Cells 1 and 31 were characterized using EDS to determine the catalyst material used. Samples were attached to a baseplate using copper tape and analyzed using magnifications between 86 and 2.0k.

Many PEM stacks use a metal-based catalyst such as platinum or boron-platinum catalysts [21, 22], vanadium-iron-platinum catalysts [23], platinum-cobalt catalysts [24, 25] lanthanide-platinum catalysts [26], platinum-beryllium oxide catalysts [27], and non-precious metal-based compounds such as Iridium, Tin, Niobium, and Iron [28, 29].

Figure 38 shows a normalized comparison of the results from the EDS scans of Cell 1 (left) and Cell 31 (right). The cathode (red) and anode (green) are stacked for each cell also for comparison. The EDS scans of the cathode material for both Cells 1 and 31 contain carbon (0.277 keV), oxygen (0.525 keV), fluorine (0.677 keV), aluminum (1.48 keV), silicon (1.73 keV), copper (8.04 keV, 8.91), and platinum (2.05 keV, 9.44 keV, and 11.07 keV). The EDS scans of the anode material for both Cells 1 and 31 contain carbon (0.277 keV), oxygen (0.525 keV), fluorine (0.677 keV), aluminum (1.48 keV), silicon (1.73 keV), copper (8.04 keV, 8.91), cobalt (6.92 keV), and platinum (2.05 keV, 9.44 keV, and 11.07 keV).

The copper was from the copper tape underneath the samples. A copper peak is not present in the Cell 31 cathode scan because the characterized portion of the sample was positioned beyond the copper tape. Finally, the silicon and aluminum were present in the samples and not detected from the baseplate. They were either originally present in the cathode and anode from the manufacturing process or were deposited through diffusion from the PEM material.

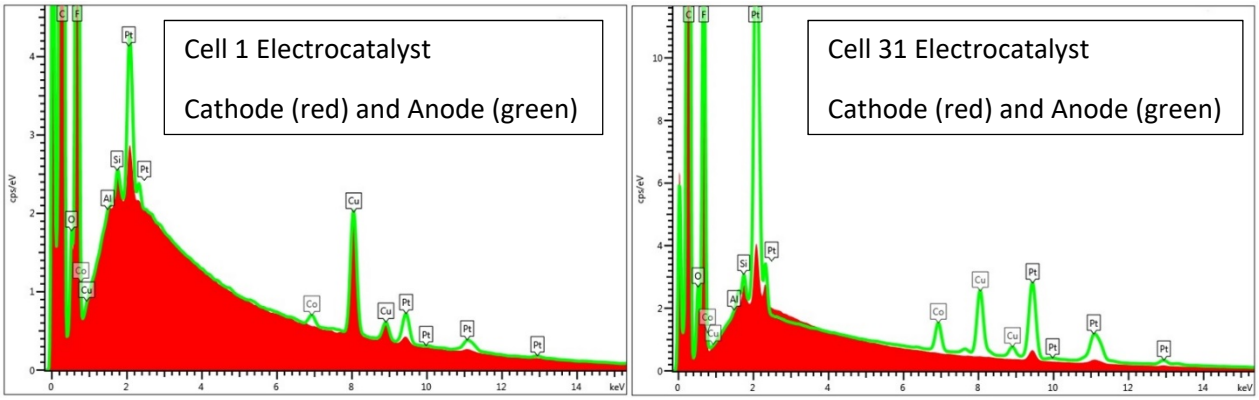

Figure 38: Cell 1 (left) and Cell 31 (right) Electrocatalyst EDS Scans for the Cathode (red) and Anode (green).

Overall, based on literature studies, the cathode contained platinum as the electrocatalyst material, while the anode contained both platinum and cobalt as its electrocatalyst material. The lack of cobalt on the cathode side (or presence of detectable cobalt on the anode side) can not be explained at this time. It could be a deliberate decision in the manufacturing process or could have resulted from the stack degradation process. An elemental mapping was performed to identify if any of the detected elements (specifically carbon, oxygen, platinum, cobalt, silicon and aluminum) could be physically located in a similar manner as the PEM material.

The location of the electrocatalyst materials and other elements can be verified using EDS elemental mapping, which would also provide information on the electrocatalyst particle size and particle size distribution. All of this information would be useful in determining if degradation changed the amount of active area of the electrocatalyst materials.

6.3. Electrocatalyst Scanning Electron Microscopy Elemental Mapping Characterization

The following information will show elemental mapping superimposed on top of SEM images for the cathode and anode electrocatalyst materials found in Cell 1 and Cell 31.

Figure 39 shows an SEM image and elemental mapping of the Cell 1 cathode (left) and anode (right) electrocatalyst materials taken at 2,000x (cathode) and 86x (anode) magnifications. The elements of carbon (red), oxygen (light green), silicon (magenta), aluminum (teal), fluorine (light blue), platinum (yellow), and cobalt (dark green) were mapped and superimposed on top of the SEM image, where applicable based on the raw EDS data.

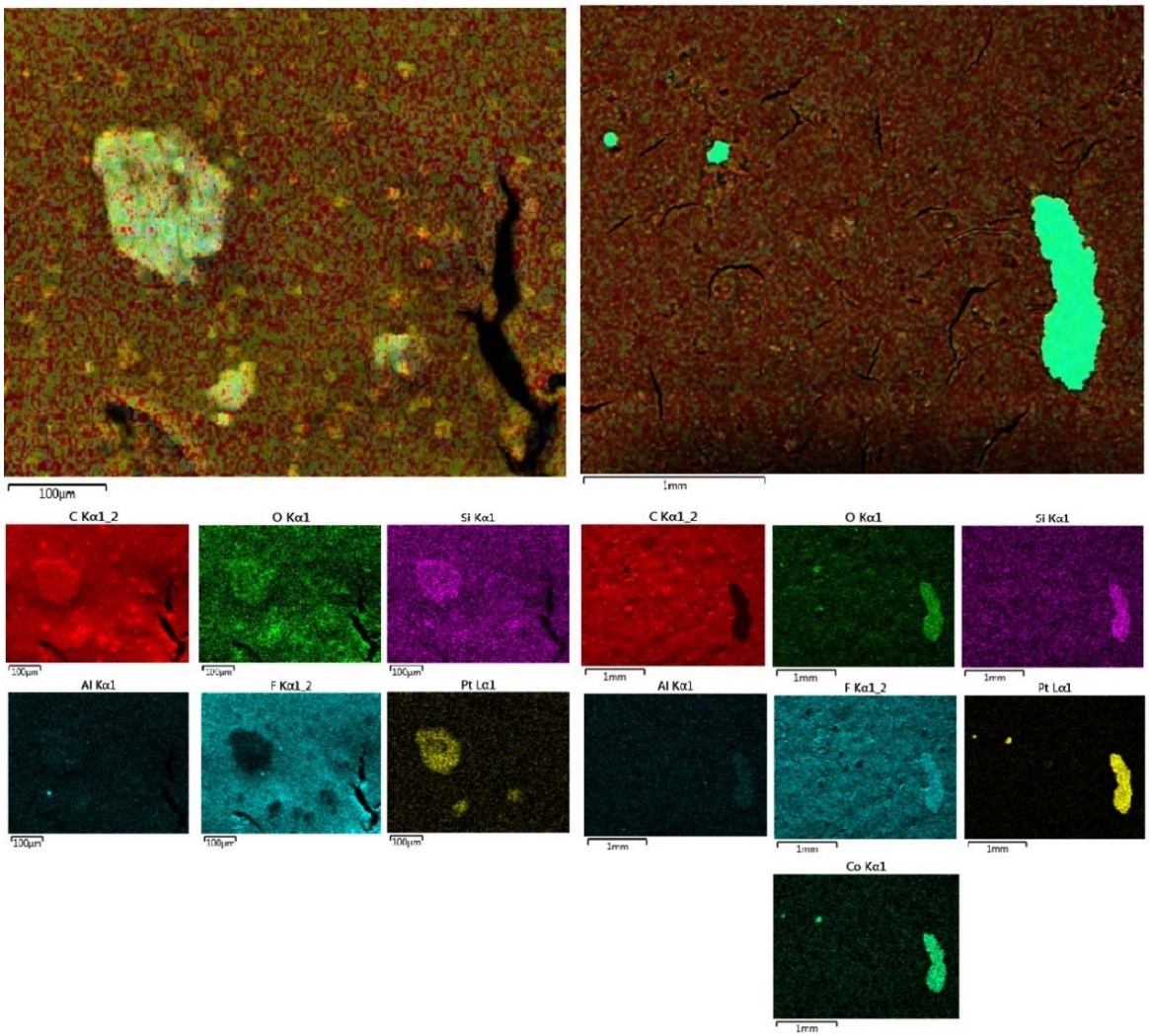

Figure 39: Cell 1 Electrocatalyst SEM Image and EDS Elemental Mapping for Cathode (left) and Anode (right). The Cathode Image was Scanned at 2,000x and the Anode at 86x Magnification. Carbon (red), Oxygen (light green), Silicon (magenta), Aluminum (teal), Fluorine (light blue), Platinum (yellow), and Cobalt (dark green). Elements are Super-Imposed on the Original SEM Image.

Figure 40 shows an SEM image and elemental mapping of the Cell 31 cathode (left) and anode (right) electrocatalyst materials both taken at 86x magnifications. The elements of carbon (red), oxygen (light green), silicon (magenta), aluminum (teal), fluorine (light blue), platinum (yellow), and cobalt (dark green) were mapped and superimposed on top of the SEM image, where applicable based on the raw EDS data.

Comparison of these two figures shows some interesting trends, which are: 1. the large particles contain increased levels of oxygen, silicon, platinum, and cobalt. Trace amounts of aluminum are present in the particles. 2. cobalt only is present on the anode side of both Cells 1 and 31 in large deposits. 3. the total area of platinum present on the cathode and anode side for Cell 1 is significantly lower than the cathode and anode area for Cell 31.

Trend 1 mentioned above can be explained by two degradation mechanisms reported in literature [30, 31] for low-temperature PEM cells. The platinum nanoparticles (and possibly the cobalt and other elements) can, over time and through multiple uses, re-deposit their material and increase their size. Reported platinum nanoparticles increase can their size to 20nm or more. A second degradation mechanism can promote soluble platinum species to re-deposit between these larger particles to bridge these particles into an even larger particle. This is what is understood to be happening to form elemental deposits that are 100um or large in size within both Cells 1 and 31.

Trend 3 could be the result of one or a combination of two different degradation mechanisms reported in literature [31]. Platinum has been shown to detach from the carbon support due to the carbon support becoming corroded or the platinum can also diffuse into the PEM material. Carbon corrosion is defined when oxides form on the surface of the carbon support. Comparison between the oxygen intensity levels, for both the cathode and anode, on Cell 1 and 31, show generally a higher level within Cell 1. This increased level of oxygen is possibly due to oxides forming on the carbon support surface, which then promotes the platinum detaching on Cell 1, which would promote even further performance reduction. If the platinum was diffusing into the PEM material then a loss in active electrolcatalyst area would result and also further reduce the stack performance. Further work will need to be completed to confirm which of these observed trends are occurring and the mechanism that promotes those results.

Now that the elemental composition and distribution of the electrocatalyst for the cathode and anode in Cells 1 and 31 was determined, a side-by-side comparison of the MEA and PEM material will be performed to investigate any effects the electrocatalyst had on the acetic acid formation.

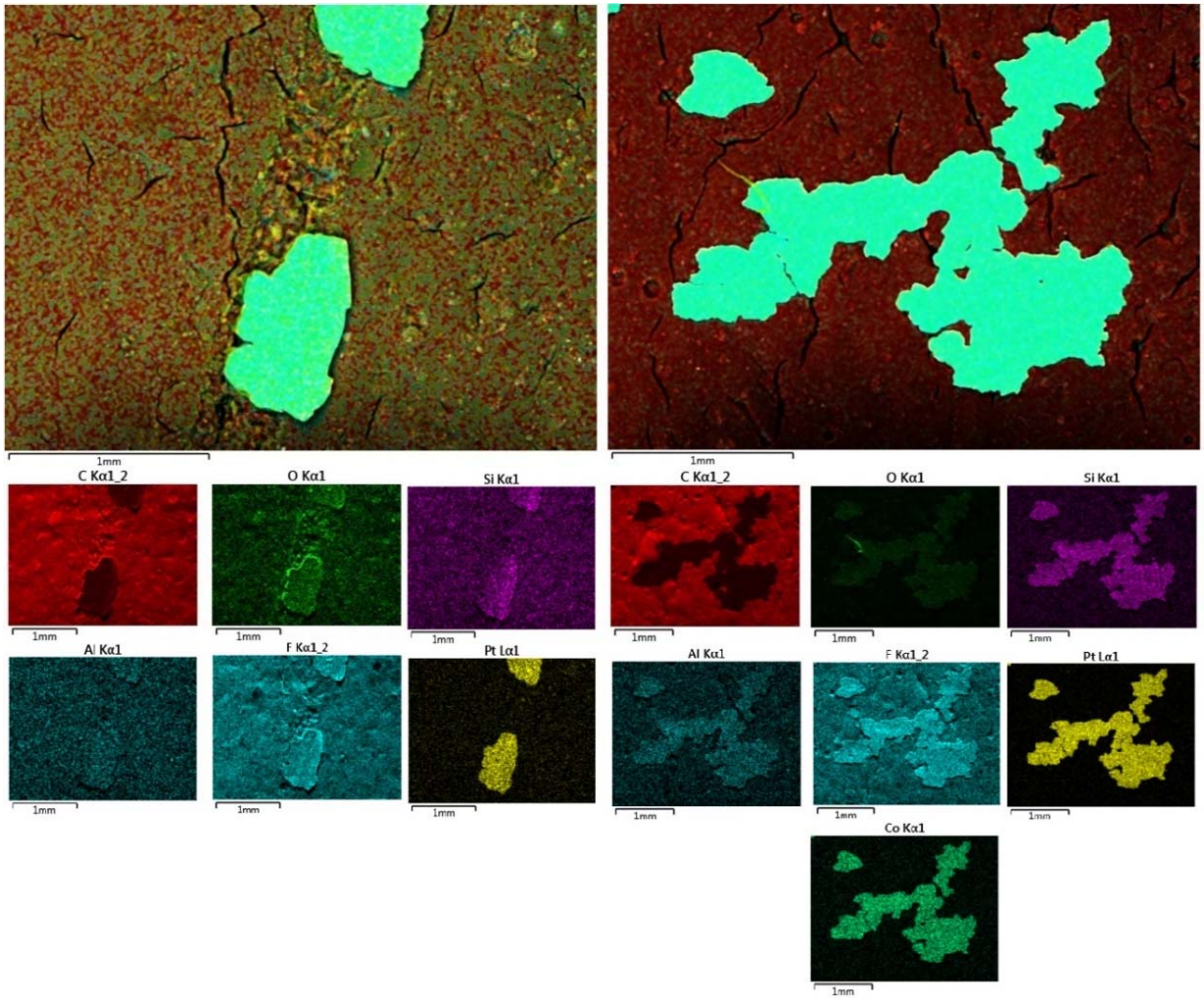

Figure 40: Cell 31 Electrocatalyst SEM Image and EDS Elemental Mapping for Cathode (left) and Anode (right). Both the Cathode Image and Anode Image were Scanned at 86x Magnification. Carbon (red), Oxygen (light green), Silicon (magenta), Aluminum (teal), Fluorine (light blue), Platinum (yellow), and Cobalt (dark green) Elements are Super-Imposed on the Original SEM Image.

6.4. PEM Fuel Cell Electrocatalyst Impact on Acetic Acid Formation

The following data will show comparisons between the MEA and PEM material samples used from Cells 1 and 31 heated at 65°C and 95°C. Samples tested when heated at room temperature did not show any noticeable differences and the FCATT PEM stack was operated at temperatures of 65°C or possibly greater.

Figure 41 shows the Cell 1 MEA (top), Cell 1 PEM material (2nd from top), Cell 31 MEA (3rd from top), and Cell 31 PEM material (bottom) chromatograms heated at 65°C in deionized water. These results are the same as what was presented in Chapter 5, except the x-axis for each chromatograph has been shortened since no compounds eluted beyond the 2.00 min point. This allows for closer analysis of the data presented.

The MEA chromatograms (which contain the electrocatalyst material), when compared to the PEM materials samples, do not show any differences in the compounds that are eluted when heated to 65°C. Temperatures well above 65°C may be required for the electrocatalyst to become stimulated and influence the acetic acid production. Even if the electrocatalyst is active at 65°C the acetic acid concentration may be too low for the GC/MS to detect it.

Figure 42 shows the Cell 1 MEA (top), Cell 1 PEM material (2nd from top), Cell 31 MEA (3rd from top), and Cell 31 PEM material (bottom) chromatograms heated at 65°C in deionized water.

The results shown in Figure 42 show that the electrocatalyst does the peak locations for acetic acid, most notably with Cell 1. When the results from the Cell 1 MEA are compared to the Cell 1 PEM material the peak area of the acetic acid dissolved in water (0.61-0.63 min) is similar in size, yet a second acetic acid peak was produced at 1.68 min with the Cell 1 MEA sample. As shown earlier in Figure 10 that second peak can be formed by a large amount of acetic acid being dissolved in the water, which saturates the water and forms as a second phase. This is not the case here, which indicates the electrocatalyst (which is the only difference between these two samples) contributed to the formation of this second peak. As with Figure 41 the amount impact of the electrocatalyst for Cell 31 heated to 95°C must not be great enough to be detected by the GC/MS equipment.

This second acetic acid peak, shown in Cell 1 heat to 95°C, corresponds to the main peak observed from the FCATT exhaust water and was what provides the pungent odor.

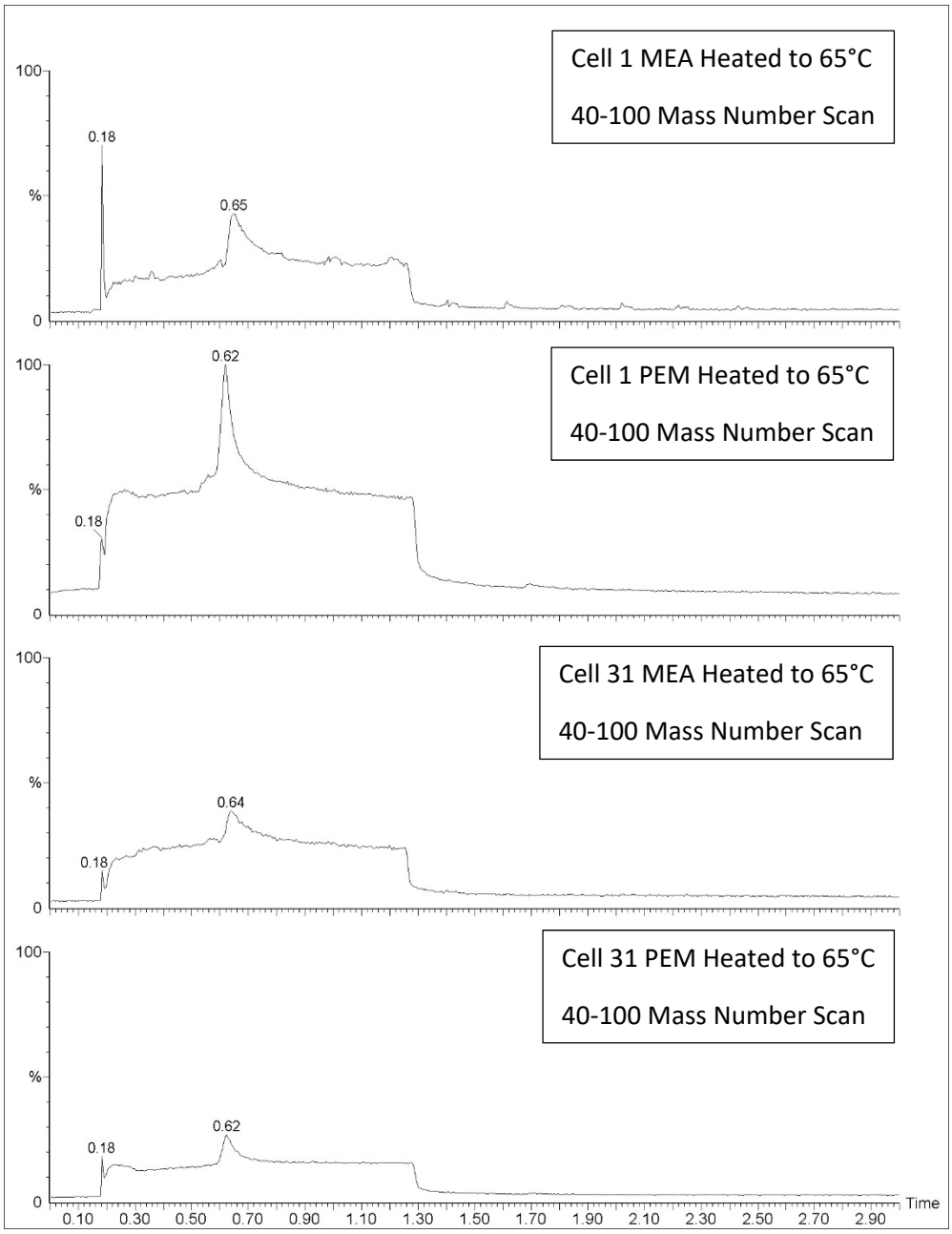

Figure 41: Cell 1 and 31 Membrane Electrode Assembly's (top and 3rd from top) Chromatograms Compared to Cell 1 and 31 Proton Exchange Membrane (2nd from top and bottom) Chromatograms Heated to 65°C.

6.5. Impact Electrocatalyst has on Acetic Acid Formation and Electrocatalyst Summary

Characterization of the electrocatalyst material and its impact on acetic acid formation showed the following information:

1. Characterization of the Cell 1 and 31 electrocatalyst material, using SEM and EDS, showed that both samples were composed of carbon support particles that contained platinum and cobalt. The platinum and cobalt were likely the electrocatalyst material.
2. The platinum and cobalt particles covered a significantly larger area on Cell 31 (for both the cathode and anode) compared to Cell 1. Cell 1 could either be losing platinum and cobalt through degradation mechanisms reported in literature where the electrocatalyst detaches from the MEA or diffuses into the PEM material. Addition work will need to be conducted to confirm which types degradation are occurring and the mechanism behind the electrocatalyst degradation.
3. Gas chromatographs of Cell 1 and 31 MEA and PEM material water samples (both heated to 65°C and 95°C) were compared to determine whether the electocatalyst had a direct impact on acetic acid formation. Comparisons showed that, under increased cell degradation and acetic acid production, the electrocatalyst will promote the formation of a second acetic acid phase that elutes around 1.70 min, and is the source of the pungent odor.

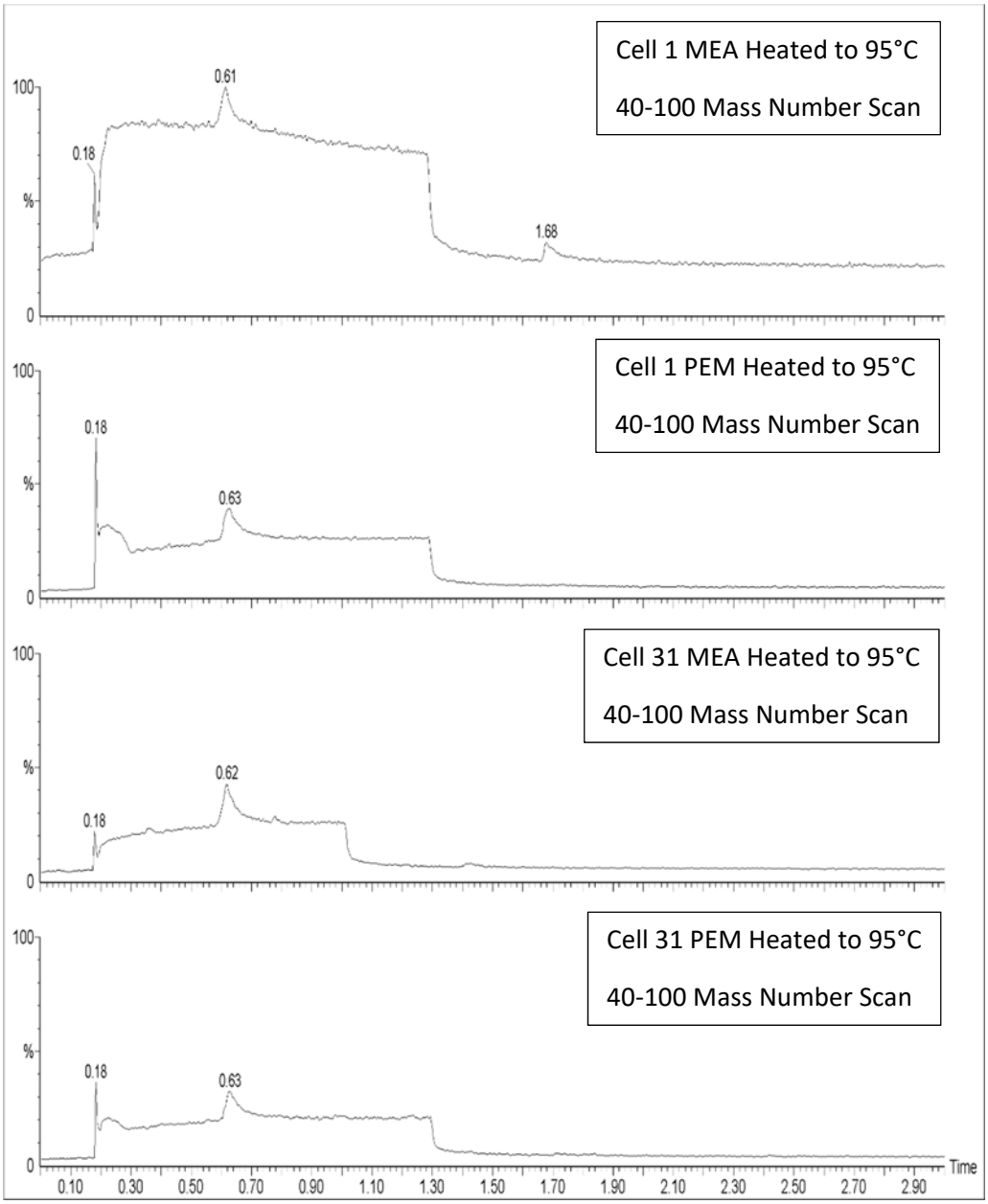

Figure 42: Cell 1 and 31 Membrane Electrode Assembly's (top and 3rd from top) Chromatograms Compared to Cell 1 and 31 Proton Exchange Membrane (2nd from top and bottom) Chromatograms Heated to 65°C.

7. FCATT PEM Stack Failure Analysis Conclusions

After extensive characterization the following conclusions can be formed as to the cause of the acetic acid production and the PEM stack performance loss:

1. The production of acetic acid was caused by the thermal degradation of the PEM fuel cell stack. The PEM material (most likely PBI) in the cell closest to the manifold (Cell 1) was found to have the largest acetic acid production. The exact mechanism for the formation of acetic acid from the PEM material is unknown at this time.
2. The cause of the PEM material in Cell 1 to thermally degrade is currently understood to be the result of the following:
    a. The manifold lowered the operating temperature of Cell 1 since it acted as a heat sink.
    b. The cell overpotential was increased due to its operating temperature being lowered. This resulted in Cell 1 having a lower cell efficiency with increased ohmic resistance losses.
    c. Cell 1 used more energy to overcome those additional ohmic resistance losses. That additional energy was lost to the PEM material as heat at the PEM/electrocatalyst interface, and started to thermally degrade and produce acetic acid in low concentrations.
    d. As the acetic acid was being formed, the electrocatalyst material was found to promote acetic acid to form a different phase which was not dissolved in the water produced by the fuel cell stack. This alternate acetic acid phase is detectable by its odor.
3. Additional indications of Cell degradation found, which possibly caused by thermal heating of PEM material interface and could lower the stack overall performance, included the following:
    a. Quartz and aluminum were identified within particles in the PEM material, which enhanced its thermal stability. The particles in Cell 1 were significantly larger than Cell 31 (200 um vs. 43 um), but larger particles did not appear to noticeable change the thermal stability of the PEM material, but given enough time, could reduce stack performance further due to reduced crystallinity in the PEM material.
    b. Platinum and cobalt electrocatalyst materials were found in both Cells 1 and 31. Both Cell 1 and 31 showed particle sizes from 100um to 1mm in size, which indicate agglomeration is occurring. The total area of platinum and cobalt particles in Cell 1 was much lower possibly due to these elements detaching themselves from the carbon support through degradation. Both agglomeration and electrocatalyst detachment will result less active area of the electrocatalyst and lower stack performance.
4. The stack as a whole was found to be operated at temperatures between 6-10°C above the manufacturer's maximum recommended operating temperature of 65°C. Based on the PEM materials sensitivity to thermal degradation, this additional heat may have resulted in the entire stack being degraded at quicker rate than originally designed.

8. References

[1] A. International, "Annual Book of ASTM Standards," 2004, pp. 1-26.

[2] M. Watanabe, H. Uchida, Y. Seki and M. Emori, "Self-Humidifying Polymer Electrolyte Membranes for Fuel Cells," *J. Electrochem. Soc.,* vol. 143, no. 12, pp. 3847-3852, 1996.

[3] I.S.Martin, A.Ursua and P. Sanchis, "Modeling of PEM Fuel Cell Performance: Steady-State and Dynamic Experimental Validation," *Energies,* vol. 7, pp. 670-700, 2014.

[4] C. KE, J. Li, X. Li, Z. Shao and B. Yi, "Protic Ionic Liquids: An Alternative Proton-Conducting Electrolyte for High Temperature Proton Exchange Membrane Fuel Cells," *RSC Adv.,* vol. 2, pp. 8953-8956, 2012.

[5] K. Mauritz and R. Moore, "State of Understanding of Nafion," *Chemical Reviews,* vol. 104, pp. 4535-4585, 2004.

[6] O.A.Baturina, S. Aubuchon and K. Wynne, "Thermal Stability in Air of Pt/C Catalysts and PEM Fuel Cell Catalyst Layers," *Chem. Mater.,* vol. 18, pp. 1498-1504, 2006.

[7] T. Blanton and R. Koestner, Characterization of Nafion Proton Exchange Membrane Films Using Wide-Angle X-Ray Diffraction, JCPDS International Centre for Diffraction Data, 2015.

[8] S. Haile, "Fuel Cell Materials and Components," *Acta Mater.,* vol. 51, pp. 5981-6000, 2003.

[9] F. Seland, T. Berning, B. Borresen and R. Tunold, "Improving the Performance of High-Temperature PEM Fuel Cells Based on PBI Electrolyte," *J. Power Sources,* vol. 160, pp. 27-36, 2006.

[10] M. Sadeghi, M. Semsarzadeh and H. Moadel, "Enhancement of the Gas Separation Properties of Polybenzimidazole (PBI) Membrane by Incorporation of Silica Nano Particles," *J. Membr. Sci.,* vol. 331, pp. 21-30, 2009.

[11] J.-W. Lee, K. Kim, S. Khan, P. Han, J. Seo, W. Jang and H. Han, "Synthesis, Characterization, and Thermal and Proton Conductivity Evaluation of 2,5-Polybenzimidazole Composite Membranes," *J. Nanomater.,* vol. 2014, pp. 1-7, 2014.

[12] D. Chen, S. Yu, M. Yang, D. Li and X. Li, "Solvent Resistant Nanofiltration Membranes Based on Crosslinked Polybenzimidazole," *RSC Adv.,* vol. 6, pp. 16925-16932, 2016.

[13] M. Han, G. Zhang, Z. Liu, S. Wang, M. Li, J. Zhu, H. Li, Y. Zhang, C. Lew and H. Na, "Cross-Linked Polybenzimidazole with Enhanced Stability for High Temperature Proton Exchange Membrane Fuel Cells," *J. Mater. Chem.,* vol. 21, pp. 2187-2193, 2011.

[14] A. Shabanikia, M. Javanbakht, H. Amoli, K. Hooshyari and M. Enhessari, "Effect of La2Ce2O7 on the Physicochemical Properties of Phosphoric Acid Doped Polybenzimidazole Nanocomposite Membranes for High Temperature Proton Exchange Membrane Fuel Cells Applications," *J. Electrochem. Soc.,* vol. 161, no. 14, pp. F1403-F1408, 2014.

[15] B. Sadeghalvad, A. Azadmehr and A. Hezarkhani, "Assessment of Iron Ore Mineral Wastes for Sulfate Removal from Groundwater Wells: A Case Study," *RSC Adv.,* pp. 1-39, 2015.

[16] A. Rajib, S. Horita, A. Rahman and A. Bakar, "Study of the Influence of Temperature on the Deposition of SiO2 Films from Reaction of Silicone Oil Vapor and Ozone Gas," *J. Sci. & Eng.,* vol. 44, pp. 1-8, 2016.

[17] N. Abeykoon, V. Garcia, R. Jayawickramage, W. Perera, J. Cure, Y. Chabal, K. Balkus and J. Ferraris, "Novel Binder-Free Electrode Materials for Supercapacitors Utilizing High Surface Area Carbon Nanofibers Derived from Immiscible Polymer Blends of PBI/6FDA-DAM:DABA," *RSC Adv.,* vol. 7, pp. 20947-20959, 2017.

[18] S. Teixeira, A. E. d. Souza, A. Pena, R. G. d. Lima and A. l. G. Miguel, Use of Charcoal and Partially Pirolsed Biomaterial in Fly Ash to Produce Briquettes: Sugercane Bagasse, 2011.

[19] S. Anandhan, K. Ponprapakaran, T. Senthil and G. George, "Parametric Study of Manufacturing Ultrafine Polybenzimidazole Fibers by Electrospinning," *Int. J. Plast. Technol.,* vol. 16, no. 2, 2012.

[20] S. Lai, J. Park, S. Cho, M. Tsai, H. Lim and K. Chen, "Mechanical Proerty Enhancement of Ultra-Thin PBI Membrane by Electron Beam Irradiation for PEM Fuel Cell," *Int. J. Hydrogen Energy.,* vol. 41, no. 22, pp. 9556-9562, 2016.

[21] A. Pullansetty, M. Subbiah and R. Sundara, "Platinum on Boron Doped Graphene as Cathode Electrocatalyst for Proton Exchange Membrane," *Int. J. Hydrog. Energy,* vol. 40, no. 32, pp. 10251-10261, 2015.

[22] J. Zhang, "Recent Advances in Cathode Electrocatalysts for PEM Fuel Cells," *Front. Energy,* vol. 5, no. 2, pp. 137-148, 2011.

[23] B. Fang, J. Luo, Y. Chen, B. Wanjala, R. Loukrakpam, J. Hong, J. Yin, X. Hu, P. Hu and C.-J. Zhong, "Nanoengineered PtVFe/C Cathode Electrocatalysts in PEM Fuel Cells: Catalyst Activity and Stability," *ChemCatChem,* vol. 3, no. 3, pp. 583-593, 2011.

[24] E. Santiagom, L. Varanda and H. Villullas, "Carbon-Supported Pt-Co Catalysts Prepared by a Modified Polyol Process as Cathodes for PEM Fuel Cells," *J. Phys. Chem.,* vol. 111, pp. 3146-3151, 2007.

[25] N. Travitsky, T. Ripenbein, D. Golodnitsky, Y. Rosenberg, L. Burshtein and E. Peled, "Pt-, PtNi- and PtCo-Supported Catalysts for Oxygen Reduction in PEM Fuel Cells," *J. Power Sources,* vol. 161, no. 2, pp. 782-789, 2006.

[26] K. Lux and E. Cairns, "Lanthanide-Platinum Intermetallic Compounds as Anode Electrocatalysts for Direct Ethanol PEM Fuel Cells," *J. Electrochem. Soc.,* vol. 153, no. 6, pp. A1139-A1147, 2006.

[27] K. Kwon, Y. Jung, H. Ku, K. Lee, S. Kim, J. Sohn and C. Pak, "CO-Tolerant Pt-BeO as a Novel Anode Electrocatalyst in Proton Exchange Membrane Fuel Cells," *Catalysts,* vol. 6, p. 68, 2016.

[28] K. Kadakia and M. Datta, "Novel (Ir.Sn,Nb)O2 Anode Electrocatalysts with Reduced Nobel Metal Content for PEM Based Water Electrolysis," *Int. J. Hydrog. Energy,* vol. 37, pp. 3001-3013, 2012.

[29] J. Chui, C. Chen, L. Grabstanowicz, D. Zhao and D.-J. Liu, "Highly Efficient Nonprecious Metal Catalyst Prepared with Metal-Organic Framwork in a Continuous Carbon Nanofibrous Network," *Proc. Natl. Acad. Sci.,* vol. 112, no. 34, pp. 10629-10634, 2015.

[30] K. Yu, D. Groom, X. Wang, Z. Yang, M. Gummalla, S. Ball, D. Myers and P. Ferreira, "Degradation Mechanisms of Platinum Nanoparticle Catalysts in Proton Exchange Membrane Fuel Cells: The Role of Particle Size," *Chem. Mater.,* vol. 26, pp. 5540-5548, 2014.

[31] Y. Shao-Horn, W. Sheng, S. Chen, P. Ferreira, E. Holby and D. Morgan, "Instability of Supported Platinum Nanoparticles in Low-Temperature Fuel Cells," *Top. Catal.,* vol. 46, no. 3-4, pp. 285-305, 2007.